Geologic and mineralogic mapping of Aram Chaos: Evidence for a water-rich history

Timothy D. Glotch and Philip R. Christensen
Department of Geological Sciences, Arizona State University, Tempe, Arizona, USA

Received 18 December 2004; revised 25 May 2005; accepted 15 June 2005; published 20 September 2005.

[1] The Aram Chaos crater on Mars contains gray, crystalline hematite within a stack of layered sediments. The Mars Global Surveyor Thermal Emission Spectrometer (MGS-TES) and Odyssey Thermal Emission Imaging System (THEMIS) were used in conjunction with data from the MGS Mars Orbital Laser Altimeter (MOLA) and the MGS Mars Orbital Camera (MOC) instruments to investigate the nature of the hematite deposits in Aram Chaos. Superposition relationships indicate that the layered sediments in Aram Chaos were deposited subsequent to the formation of the chaotic terrain. This observation, along with the possible detection of sulfates and relatively high abundance of phyllosilicates associated with the layered units in Aram Chaos, provides evidence for the formation of the hematite-bearing units in Aram Chaos in a water-rich environment. Although there are several similarities between the hematite-bearing units in Aram Chaos and Meridiani Planum, an estimated age difference of 0.7–1.0 Gyr exists between them. This indicates that either a stable, thick atmosphere was present well into the Hesperian, or, more likely, that episodic catastrophic release of water provided a temporary environment for deposition of the Aram Chaos hematite unit similar to what existed for the deposition of the Meridiani Planum hematite unit close to 1 Gyr earlier.

Citation: Glotch, T. D., and P. R. Christensen (2005), Geologic and mineralogic mapping of Aram Chaos: Evidence for a water-rich history, *J. Geophys. Res.*, *110*, E09006, doi:10.1029/2004JE002389.

1. Introduction

[2] Aram Chaos is a 280 km diameter crater centered at 2.5°N, 338.5°E. Like craters in Meridiani Planum and Arabia Terra, it has been filled with a large amount of material since its formation [*Malin*, 1976; *Christensen et al.*, 2001a; *Edgett and Malin*, 2002]. The interior deposits of this crater differ substantially in two ways from those of other craters in the area. First, Aram Chaos contains the second-largest known deposit of gray hematite on Mars, with an areal coverage of ~5000 km^2 [*Christensen et al.*, 2001a]. Second, the sedimentary units in the interior of the crater are capped by a light-toned unit [*Catling and Moore*, 2003] that has a higher thermal inertia than the underlying sedimentary units [*Glotch and Christensen*, 2003].

[3] Aram Chaos is connected to the Ares Vallis outflow channel by 15 km wide, 2.5 km deep channel through which material flowed outward from Aram Chaos to Ares Vallis. The association of Aram Chaos with the outflow channels, its basin morphology, the presence of friable sedimentary layers, and the occurrence of gray, crystalline hematite may be indicative of past surface and/or subsurface liquid water in the region. In this paper, we present a model of the geologic history of Aram Chaos and the formation of the gray hematite in the region.

0148-0227/05/2004JE002389

2. Background

2.1. Hematite Formation

[4] Upon the initial discovery of gray hematite by the Mars Global Surveyor (MGS) Thermal Emission Spectrometer (TES) instrument, *Christensen et al.* [2000a, 2001a] proposed five methods for formation of gray hematite on Mars: (1) low-temperature precipitation of Fe-oxides/hydroxides from standing, oxygenated, Fe-rich water, followed by subsequent alteration to gray hematite, (2) low-temperature leaching of Fe-bearing silicates and other materials leaving an Fe-rich residue (laterite-style weathering) which was subsequently altered to gray hematite, (3) direct precipitation of gray hematite from Fe-rich circulating fluids of hydrothermal or other origin, (4) formation of gray hematite surface coatings during subareal weathering, and (5) thermal oxidation of magnetite-rich lavas. Of these models, leaching and weathering processes generally produce red, rather than gray, hematite, and oxidation of a magnetite-rich lava was considered unlikely due to the lack of lava flow features. Therefore *Christensen et al.* [2000a, 2001a] favored either an aqueous deposition model or a hydrothermal deposition mechanism for the formation of the gray hematite.

[5] Subsequent to the initial description of the hematite-rich regions, several workers conducted detailed spectral, geomorphic, and geochemical studies to assess different models of gray hematite formation. *Lane et al.* [2002] investigated the infrared spectral properties of a variety of naturally occurring hematite samples. Their results indicate that the lack of an absorption band at 390 cm^{-1} in the MGS-TES hematite spectrum is evidence for platy hematite grains. They proposed a model in which an ancient iron oxide or hydroxide formation was buried and excavated in recent times and the hematite seen today is the result of burial metamorphism or primary deposition under stress of the original iron oxide deposit.

[6] Several authors [*Noreen et al.*, 2000; *Chapman and Tanaka*, 2002; *Hynek et al.*, 2002; *Arvidson et al.*, 2003] have favored a volcanic origin for the hematite-bearing deposits. *Noreen et al.* [2000] proposed a model involving the oxidation of magnetite in ignimbrites and suggested the El Laco volcanic iron oxide deposits in Chile as a possible analog. As *Catling and Moore* [2003] point out, however, most of the oxide deposits at El Laco are still magnetite, not hematite, and no magnetite has been detected in the Martian hematite exposures [*Christensen et al.*, 2001a]. *Chapman and Tanaka* [2002] expanded on the idea of a volcanic origin for the hematite, attributing the hematite mineralization to alteration of volcanic ash by an Fe-rich hydrothermal fluid. They related the hematite mineralization to geomorphic features over Margaritifer, Xanthe, and Merridiani Terrae and argue for widespread magma-ice interactions.

[7] *Catling and Moore* [2003] noted that the oxygen fugacity at the Martian surface is too low to thermally oxidize a magnetite-rich lava to hematite. Instead, based on geochemical modeling and a study of the geology of Aram Chaos, they concluded that hematite formed underground at a temperature greater than 100°C in a hydrothermally charged aquifer. *Hynek et al.* [2002] performed a geomorphic analysis of the Meridiani Planum area, and based on geomorphic evidence, also favored a secondary hydrothermal emplacement mechanism for the hematite, although they leave open the possibility of oxidation of magnetite-rich volcanic materials. *Christensen and Ruff* [2004], however, arrived at a different conclusion after examining geomorphic evidence and TES data. Their work provides evidence for a subaqueous origin for the hematite-bearing deposits in Meridiani Planum. This is supported by evidence for an ancient multiringed impact structure interpreted by *Newsom et al.* [2003] as a paleolake basin. Recently, *Hynek* [2004] inferred, based on the large areal extent of a light-toned etched unit, that surface or near surface water was present over a large area of Mars for an extended period of time. Along these lines, *Calvin et al.* [2003] and *Fallacaro and Calvin* [2003] preferred a model of deposition analogous to terrestrial banded iron formation (BIF) deposits, which would have involved abundant water. By contrast, *Kirkland et al.* [2004] argued that the deposits in Meridiani Planum are composed of fine intimate hematite, possibly in the form of coatings, a process that does not necessarily involve abundant water. *Ormö et al* [2004] suggested that the combination of light-toned deposits and hematite seen in Meridiani Planum and Aram Chaos may be analogous to bleached beds and hematite concretions seen in southern Utah [*Chan et al.*, 2000, 2004], where the presence of hematite is determined by preferential fluid flow in strata of variable permeability. Finally, it has also been suggested that phosphate adsorption onto iron oxide crystals may have played an important role in the aqueous formation of Martian hematite [*Barron et al.*, 2004; *Greenwood et al.*, 2004].

[8] *Glotch et al.* [2004] examined emissivity spectra from a large suite of synthetic and natural hematite samples. This study showed that spectra of magnetite-derived and high-temperature hydrothermal hematite provide poor fits to the Martian hematite spectrum. The best fit to the Martian hematite spectrum was hematite derived from goethite under dry conditions at 300°C in the laboratory. Spectra of goethite-derived hematite formed at lower temperatures are dominated by emission parallel to the [001] axis. This is consistent with the Martian thermal emission hematite spectrum [*Lane et al.*, 2002]. Although the lowest temperature at which goethite was dehydroxylated to hematite by *Glotch et al.* [2004] was 300°C, the goethite dehydroxylation process occurs easily at lower temperatures ($\leq$100°C) in nature [*Cornell and Schwertmann*, 1996]. The experiments performed by *Glotch et al.* [2004] were under dry conditions, and kinetic crystal growth effects in aqueous environments cause the dehydroxylation temperature of goethite to be reduced substantially [*Cornell and Schwertmann*, 1996; *De Grave et al.*, 1999]. It has been suggested that goethite may be unstable relative to hematite under nearly all geologic conditions [*Berner*, 1969; *Langmuir*, 1971].

[9] The results from the Mars Exploration Rover Opportunity [*Squyres et al.*, 2004; *Christensen et al.*, 2004a] have provided evidence that, at least in Meridiani Planum, the formation of hematite involved an aqueous mechanism. Hematite at Meridiani Planum consists chiefly of spherules interpreted as concretions that have weathered out of a sulfate-rich outcrop. In addition, hematite is also a component of the outcrop matrix material. Cross-bedding textures within the outcrop [*Squyres et al.*, 2004] indicate subaqueous deposition. It is likely that the formation of the hematite concretions occurred as a result of postdepositional aqueous alteration of the outcrop. The Mössbauer spectrometer [*Klingelhöfer et al.*, 2003] identified jarosite as a component of the outcrop, and goethite and jarosite are often associated in nature [*Herbert*, 1995, 1997] and are easily coprecipitated in the laboratory [*Brown*, 1971; *Stahl et al.*, 1993] The details of possible processes for conversion of goethite to hematite on Mars have been discussed by *Glotch et al.* [2004]. The kinetics of the conversion process favor an aqueous environment over a dry one.

2.2. Formation of Chaotic Terrain

[10] Chaotic terrain was first recognized in Mariner 6 imagery [*Sharp et al.*, 1971] and described in detail from Mariner 9 imagery [*Sharp*, 1973]. Its main characteristic features are a rough floor topography, large (up to tens of kilometers) slumped and angled blocks, and often large arcuate fractures that extend to the surrounding plains [*Sharp*, 1973]. It was recognized that the fracture pattern in the chaotic terrain was indicative of removal of subsurface material, and three possible mechanisms for the removal of this material were offered: (1) dissolution of subsurface rock materials, (2) the melting of ground ice,

and (3) the evacuation of magma by volcanism [*Sharp*, 1973]. Of these methods, the last two have been given the most consideration. Several authors have argued for melting of a permafrost layer by a volcanic intrusion, causing subsequent collapse [*Maxwell and Picard*, 1974; *Masursky et al.*, 1977]. *Chapman and Tanaka* [2002] favored a volcanic eruptive origin for the formation of at least some chaotic terrains, and *Carr* [1979] proposed a model in which a high-pressure confined aquifer forms below a permafrost layer. If the pressure of the confined aquifer exceeds the effective lithostatic pressure, then the aquifer could be released in a catastrophic event. The dissolution of subsurface carbon dioxide or methane clathrate hydrates could also lead to catastrophic release of subsurface water [*Milton*, 1974; *Komatsu et al.*, 2000; *Max and Clifford*, 2000]. Alternatively, *Nummedal* [1978] proposed that a seismic event could cause a catastrophic release of water due to the subsurface liquefaction of a sedimentary unit. *Nummedal and Prior* [1981] further suggested that resulting debris flows are responsible for the formation of the chaotic terrain and the large outflow channels associated with many of them. Likely locations for Martian debris flows have been the subject of numerous studies [*Tanaka*, 1988; *Rotto and Tanaka*, 1991; *Tanaka*, 1999; *Tanaka et al.*, 2001]. Regardless of the exact mechanism, it appears likely that subsurface water was present during the formation of most chaotic terrains.

3. Methods

3.1. Instrument Descriptions

[11] The main data sets used in this study are from the MGS-TES and Odyssey-THEMIS instruments. Images from the MGS-Mars Orbital Camera (MOC) *Malin et al.* [1991, 1992] provide high-resolution views of surface morphology. Topographic data from the MGS-Mars Orbiter Laser Altimeter (MOLA) [*Zuber et al.*, 1992; *Smith et al.*, 2001] were also used to determine the stratigraphy and structure of the Aram Chaos units.

3.1.1. TES

[12] The MGS-TES instrument is a Fourier-Transform Michelson Interferometer (FTIR) that covers the wave number range from ~1700 to 200 cm^{-1} (~6 to 50 μm) at 5 or 10 cm^{-1} spectral sampling. Each detector has an instantaneous field of view of ~8.5 mrad, providing a spatial resolution of ~3 by 3 km. From the final TES mapping orbit of ~380 km, the actual surface sampling is 3 × ~8 km. The pixels are elongated downtrack because the final mapping orbit of MGS is in the opposite direction of that originally planned, and the image motion compensation could not be used. MGS-TES also has two broadband radiometers, which measure energy in the thermal (~5–100 μm) and visible/near-infrared (~0.3–3.5 μm) wavelengths. The focal planes in each wavelength interval consist of 6 detectors arranged in a 3 by 2 array. For a complete description of the TES instrument and instrument operations, see *Christensen et al.* [1992, 2001b].

3.1.2. THEMIS

[13] The Mars Odyssey THEMIS instrument contains both thermal infrared (TIR) and visible/near-infrared (VNIR) imagers [*Christensen et al.*, 2004b]. The THEMIS TIR imager consists of an uncooled 320 by 240 microbolometer array with 9 spectral channels centered from 6.5 to 15 μm. Spatial sampling is 100 m from the 420 km altitude circular orbit of the Mars Odyssey spacecraft. An internal calibration flag and instrument response functions determined from prelaunch data are used to produce calibrated radiance images. The THEMIS VNIR imager is a frame imager that consists of five spectral bands centered between 425 and 860 nm. Spatial sampling is 18 m, and pixels can be coadded to decrease bandwidth. For a complete description of random and systematic uncertainties, see *Christensen et al.* [2004b] and *Bandfield et al.* [2004].

3.2. Mapping Methods

[14] Detailed mapping of the Aram Chaos region of Mars (latitude 0° to 5°N, longitude 336°E to 341°E) was performed using Mars Odyssey THEMIS daytime infrared (Figure 1a) and nighttime infrared (Figure 1b) mosaics as a base. High-resolution (18 m/pixel) and moderate-resolution (36 m/pixel) THEMIS visible imagery and MGS-MOC narrow-angle images were also inspected. MGS-TES data were used to map albedo at 32 pixels per degree (ppd) and hematite abundance for individual TES detectors. The hematite map was then overlain onto the THEMIS mosaic base (Figure 2), taking into account the eastward longitude shift of 0.271° from the MGS and Odyssey cartographic systems [*Rogers et al.*, 2005]. The 128 ppd Mars Orbital Laser Altimeter (MOLA) gridded topography data were used to generate shaded relief and 100 m contour maps. Individual MOLA profiles were also inspected. Definition of map units in Aram Chaos was mainly geomorphic in nature, although lithostratigraphic properties, including mineralogy and thermal inertia derived from TES, TES albedo, and THEMIS-derived surface temperature were also used.

[15] TES data from OCKs 1583 through 7000 were used to determine the surface mineralogy of the units mapped in this study. (OCK 1683 is equivalent to MGS mapping orbit 1; some science phasing orbit data were used in this study.) Only spectra that had low atmospheric dust and water ice components, as determined by the TES data [*Smith et al.*, 2000a, 2000b] were used. The deconvolution method of atmospheric removal [*Smith et al.*, 2000a] was performed to isolate the surface component of the TES emissivity spectrum, and a linear deconvolution [*Ramsey and Christensen*, 1998] analysis was performed on the resulting surface spectra to determine the surface mineralogy. Spectra from orbits with similar atmospheric conditions representing the mapped surface units were averaged previous to the surface-atmosphere separation. These were then combined with averages from other orbits over the same surface units subsequent to the surface-atmosphere separation to increase the signal-to-noise ratio.

[16] Three spectral libraries (Table 1) were used in the deconvolution analysis of TES data. The reported modal mineralogy (Table 2) for each unit is the average of results from deconvolution analyses with each of the three libraries. The first library used is similar to that used by *Bandfield* [2002]. It contains 32 mineral end-members and 6 atmospheric end-members. [*Glotch et al.*, 2002] reported that deconvolving with a hematite end-member that is a poor spectral match to the observed

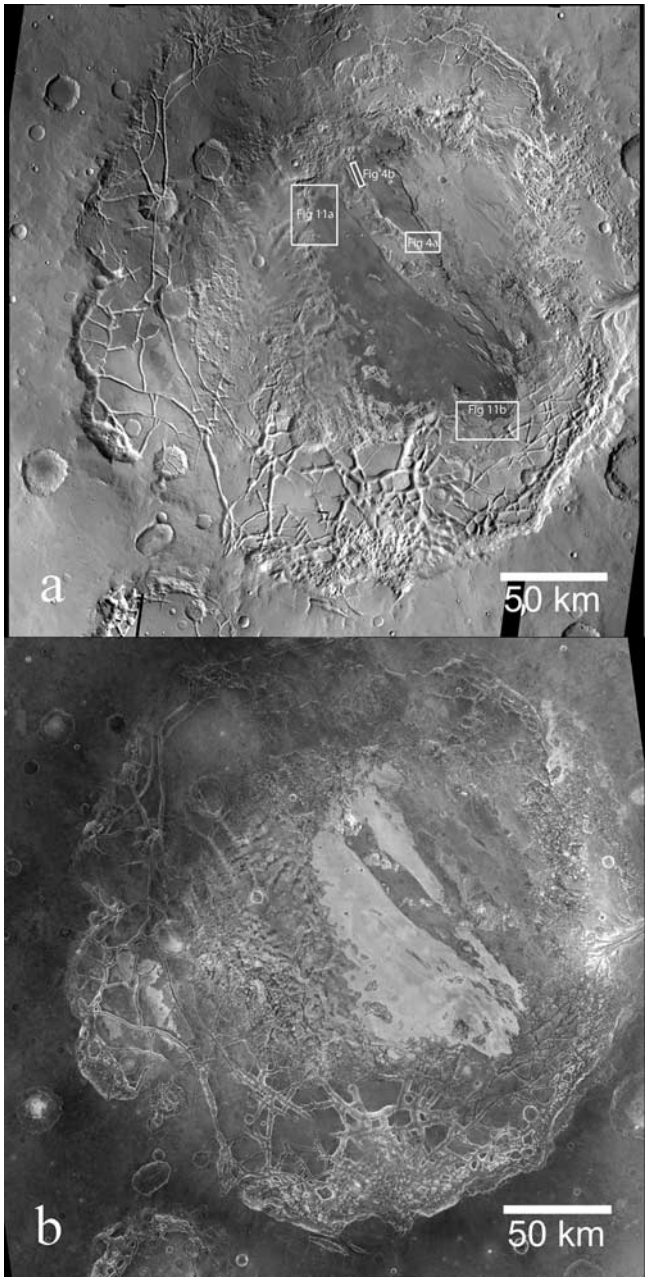

Figure 1. THEMIS mosaics of the Aram Chaos region. In both images, darker tones represent cooler surfaces and brighter tones indicate warmer surfaces. (a) Daytime infrared band 9 radiance mosaic. (b) Nighttime infrared band 9 radiance mosaic.

TES spectrum can result in the overmodeling of sulfate and olivine in a deconvolution analysis. Therefore the hematite end-member used by *Bandfield* [2002] has been replaced by the target transformation-derived hematite spectrum [*Glotch et al.*, 2004] that was recovered from the TES data. The second library is similar to the first, although the basaltic glass end-member was replaced with a pure SiO_2 glass [*Wyatt et al.*, 2001], several additional sulfate end-members provided by A. Baldridge (personal communication, 2004), and the TES-derived global high-albedo surface [*Bandfield and Smith*, 2003] were added. The third library builds upon the second by adding six smectite clay spectra [*Michalski et al.*, 2005].

4. Mapping Results

4.1. Unit Overview

[17] The types of terrain present in Aram Chaos can be divided into two classes (disrupted and nondisrupted) based on the presence or absence of fractures. The disrupted, or chaotic units fall into three subunits defined here as Fractured Plains, High Thermal Inertia Chaotic Terrain, and Knobby Terrain. Fractured Plains and Knobby Terrain were defined previously by *Schultz et al.* [1982], although the Knobby Terrain described there has been further subdivided into several units for this study. Specifically, the Knobby Terrain of *Schultz et al.* [1982] was divided into several sedimentary units characterized by their composition, the presence or absence of hematite, and their geomorphologic characteristics. The nondisrupted units are divided into the Cap Unit, the Primary Hematite Unit, the Subdued Unit, the Secondary Hematite Unit, the Non-Hematite Layered Unit, and the Outflow Plains Unit. In the following descriptions, each unit is assigned as either a disrupted chaotic unit (C), or a nondisrupted plains unit (P).

4.2. Map Unit Descriptions

[18] A map and schematic cross section of Aram Chaos divided into the following units is shown in Figure 3.

[19] 1. The *Cap Unit* (P_c) was first described by *Catling and Moore* [2003] using MOC wide-angle and narrow-angle images, and was mapped as part of the more extensive Ares Unit by *Tanaka and Skinner* [2004]. *Catling and Moore* [2003] described this unit as "light-toned" based on MOC imagery. TES albedo shows that this unit is indeed lighter than the surrounding units. It has an albedo that ranges from 0.165 to 0.18, as opposed to 0.12 to 0.13 for the surrounding units. High-resolution THEMIS visible images and MOC images show a heavily etched surface that traps dark sand (Figure 4). THEMIS infrared imagery shows this unit is cool in the daytime and warm at night relative to its surroundings (Figure 1), indicating that it has a relatively high thermal inertia. Low-resolution TES-derived thermal inertia [*Jakosky et al.*, 2000; *Mellon et al.*, 2000] of the unit varies from ~400 to 500 (units of $Jm^{-2}s^{-1/2}K^{-1}$ used throughout) compared to values between 270 and 350 for the other layered units. These values correspond to surfaces with uniform unconsolidated particle sizes of 2.4–7 and ~0.7–1.6 mm respectively [*Presley and Christensen*, 1997]. Alternatively, P_c is more cemented or has a higher abundance of clasts and rocks than the surrounding units [*Christensen et al.*, 2003]. P_c appears to have an unusual erosion pattern characterized by the formation of cliff faces, jagged contacts with the surrounding terrain, and several outliers from the two main occurrences that suggest the unit was once more extensive (Figure 5).

[20] 2. The major component of the *Primary Hematite Unit* (P_h) is basaltic sand, with a hematite abundance that varies between 10 and 15% [*Christensen et al.*, 2001a]. P_h has a thickness of 100–150 m and appears to be easily erodable. THEMIS visible imagery combined with the TES-derived hematite abundance map and 128 ppd MOLA

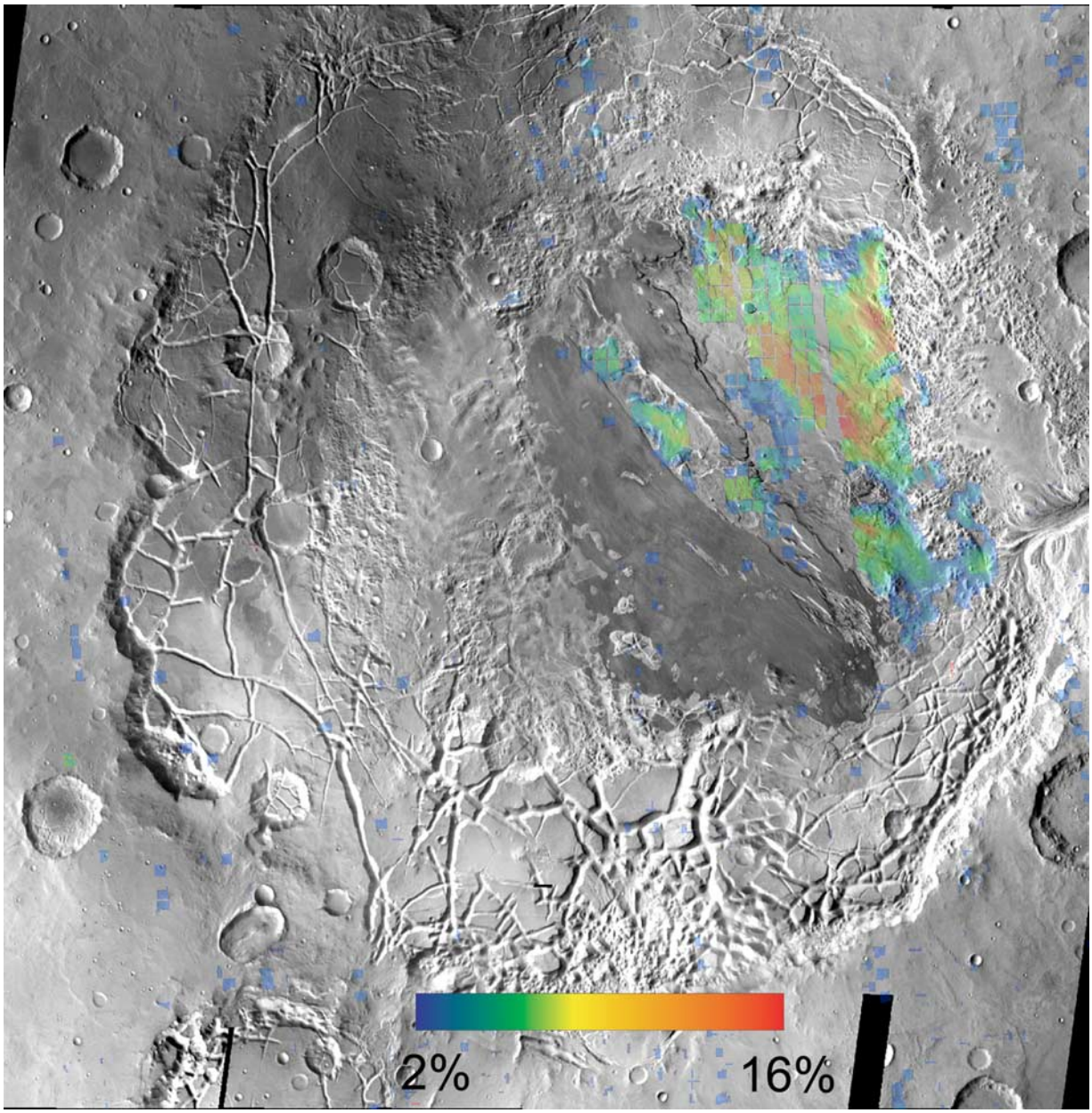

Figure 2. Hematite abundance overlaid on a daytime infrared band 9 radiance mosaic. Hematite abundance ranges from 0 to ~16%.

gridded topography shows that the highest concentrations of crystalline hematite are confined to a single, well-defined layer about 100–150 m thick (Figure 6). The layers stratigraphically below this unit have lower hematite abundances (Figure 6) indicating that this unit is enriched in hematite and that the hematite is not simply accumulating in a topographic low. P_h may be the source for hematite transported downslope onto lower units.

[21] The TES-derived thermal inertia of the hematite rich layer varies between ~280 and 315, implying either a finer particle size or less consolidation than P_c. For comparison, thermal inertia values for the hematite-bearing unit in Meridiani Planum range from ~170–240, suggesting that the Aram unit has either more rocks or coarser clasts than the sand and spherule-rich surface at Meridiani Planum [*Squyres et al.*, 2004; *Bell et al.*, 2004, *Soderblom et al.*, 2004].

[22] 3. The *Subdued Terrain* (P_s) unit lies directly below P_c in the west central portion of Aram Chaos, and in some areas, appears to crop out as erosional windows through P_c (Figure 7). Unlike unit P_h, which also appears to outcrop directly below P_c, this unit has no detectable hematite (Table 2). The typical thermal inertia of this unit ranges from 330 to 350. Features consistent with fractured chaotic terrain appear within the unit, but they are muted, and this unit does not have a high thermal inertia like the chaotic units in Aram Chaos.

[23] 4. Unlike P_h, the *Secondary Hematite Unit* (P_{h2}) is not confined to a single well-defined layer. It is characterized by a lower concentration of gray hematite relative to

Table 1. Mineral End-Members From the Three Spectral Libraries Used in This Study

Library 1	Library 2	Library 3
Quartz BUR-4120	Quartz BUR-4120	Quartz BUR-4120
Microcline BUR-3460	Microcline BUR-3460	Microcline BUR-3460
Albite WAR-0244	Albite WAR-0244	Albite WAR-0244
Oligoclase BUR-060D	Oligoclase BUR-060D	Oligoclase BUR-060D
Andesine BUR-240	Andesine BUR-240	Andesine BUR-240
Labradorite WAR-4524	Labradorite WAR-4524	Labradorite WAR-4524
Bytownite WAR-1384	Bytownite WAR-1384	Bytownite WAR-1384
Anorthite BUR-340	Anorthite BUR-340	Anorthite BUR-340
Actinolite HS-116.4B	Actinolite HS-116.4B	Actinolite HS-116.4B
Biotite BUR-840	Biotite BUR-840	Biotite BUR-840
Muscovite WAR-5474	Muscovite WAR-5474	Muscovite WAR-5474
Chlorite WAR-1924	Chlorite WAR-1924	Chlorite WAR-1924
Enstatite HS-9.4B	Enstatite HS-9.4B	Enstatite HS-9.4B
Bronzite NMHN-93527	Bronzite NMHN-93527	Bronzite NMHN-93527
Diopside WAR-6474	Diopside WAR-6474	Diopside WAR-6474
Augite NMNH-9780	Augite NMNH-9780	Augite NMNH-9780
Augite NMNH-122302	Augite NMNH-122302	Augite NMNH-122302
Hedenbergite, DSM-HED01	Hedenbergite, DSM-HED01	Hedenbergite, DSM-HED01
Serpentine HS-8.4B	Serpentine HS-8.4B	Serpentine HS-8.4B
Serpentine BUR-1690	Serpentine BUR-1690	Serpentine BUR-1690
Forsterite AZ-01	Forsterite AZ-01	Forsterite AZ-01
Fayalite WAR-RGFAY01	Fayalite WAR-RGFAY01	Fayalite WAR-RGFAY01
Hematite (TT-Derived)[a]	Hematite (TT-Derived)[a]	Hematite (TT-Derived)[a]
Anhydrite ML-S9	Anhydrite ML-S9	Anhydrite ML-S9
Gypsum ML-S6	Gypsum ML-S6	Gypsum ML-S6
Calcite C27	Calcite C27	Calcite C27
Dolomite C28	Dolomite C28	Dolomite C28
Nontronite WAR-5108g granular	Nontronite WAR-5108g granular	Nontronite WAR-5108g granular
Fe-smectite SWa-1s	Fe-smectite SWa-1s	Fe-smectite SWa-1s
Illite IMt-2g granular	Illite IMt-2g granular	Illite IMt-2g granular
SiK Glass MW-SiK-GLASS	SiK Glass MW-SiK-GLASS	SiK Glass MW-SiK-GLASS
Basaltic Glass VEHBGLAS	SiO2 Glass MW-SiO2-GLASS	SiO2 Glass MW-SiO2-GLASS
	High Albedo Surface[b]	High Albedo Surface[b]
	Bassanite ML-S7	Bassanite ML-S7
	Epsomite 1[c]	Epsomite 1[c]
	Epsomite 2[c]	Epsomite 2[c]
	Epsomite 3[c]	Epsomite 3[c]
	MgSO4 1[c]	MgSO4 1[c]
	MgSO4 2[c]	MgSO4 2[c]
		Sbdl < 0.2 μm[d]
		Nau-1 < 0.2 μm[d]
		Nau-2 < 0.2 μm[d]
		SHca < 0.2 μm[d]
		Swy-1 < 0.2 μm[d]
		Saponite < 0.2 μm[d]

[a] *Glotch et al.* [2004].
[b] *Bandfield and Smith* [2003].
[c] A. Baldridge (2004).
[d] *Michalski et al.* [2005].

P_h, with the mineralogy of the other components being similar. The secondary hematite is not associated with any set of layers, but covers layered terrains with an irregular boundary over an elevation difference of ~500 m with thermal inertia values varying from ~270 to 340. This, along with the fact that hematite is present in low concentrations in nearby low-elevation chaotic terrains (Figure 3) suggests that this is a surficial unit of transported hematite that mantles older rock units.

[24] 5. The *Non-Hematite Layered Unit* (P_{nh}) lies stratigraphically below P_h. It appears geomorphologically identical to P_h, but has a thermal inertia of ~330, which is higher than the thermal inertia range determined for P_h. Deconvolution of TES data indicate that this unit contains no hematite and is mineralogically similar to unit Ps. From a geomorphologic standpoint, P_{nh} appears to be thicker and has better defined layers than P_s, through which chaotic fractures are observed.

[25] 6. The *Outflow Plains Unit* (P_o) occurs exclusively at the eastern margin of the crater, where a 15 km wide channel flows outward from Aram Chaos and into Ares Vallis. It is characterized by deep (200–300 m) tributaries feeding the outflow channel and eroded terraces at the crater rim.

Table 2. Derived Surface Mineralogies of Six Spectral Units in Aram Chaos

Component	Cap Unit	Hematite Unit	Subdued Unit	Layered Terrain	Chaotic Terrain	Basaltic Sand
Plagioclase	20	20	30	30	35	35
Pyroxene	30	15	25	20	40	30
Hematite	0	15	0	5	0	5
Sulfate	10	10	10	10	5	5
Carbonate	15	15	15	15	10	10
Glass/Phyllosilicate	20	25	20	20	5	15
Other	5	0	0	0	5	0

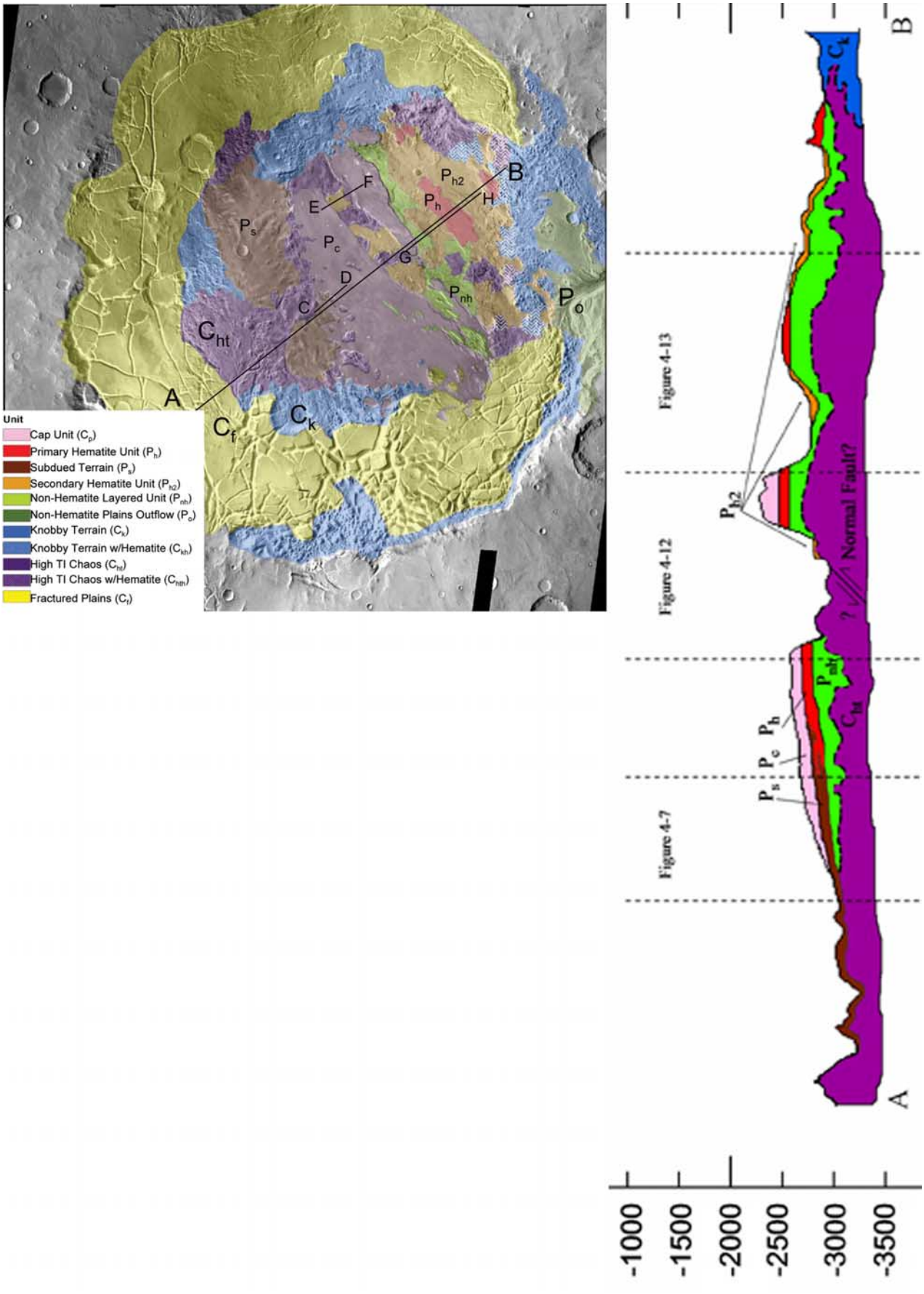
A
B
C
D
E
F
G
H
P_{h2}
P_h
P_s
P_c
P_{nh}
P_o
C_{ht}
C_f
C_k
Unit
Cap Unit (C_p)
Primary Hematite Unit (P_h)
Subdued Terrain (P_s)
Secondary Hematite Unit (P_{h2})
Non-Hematite Layered Unit (P_{nh})
Non-Hematite Plains Outflow (P_o)
Knobby Terrain (C_k)
Knobby Terrain w/Hematite (C_{kh})
High TI Chaos (C_{ht})
High TI Chaos w/Hematite (C_{hth})
Fractured Plains (C_f)
Figure 4-13
Figure 4-12
Figure 4-7
Normal Fault?
-1000
-1500
-2000
-2500
-3000
-3500

Figure 3

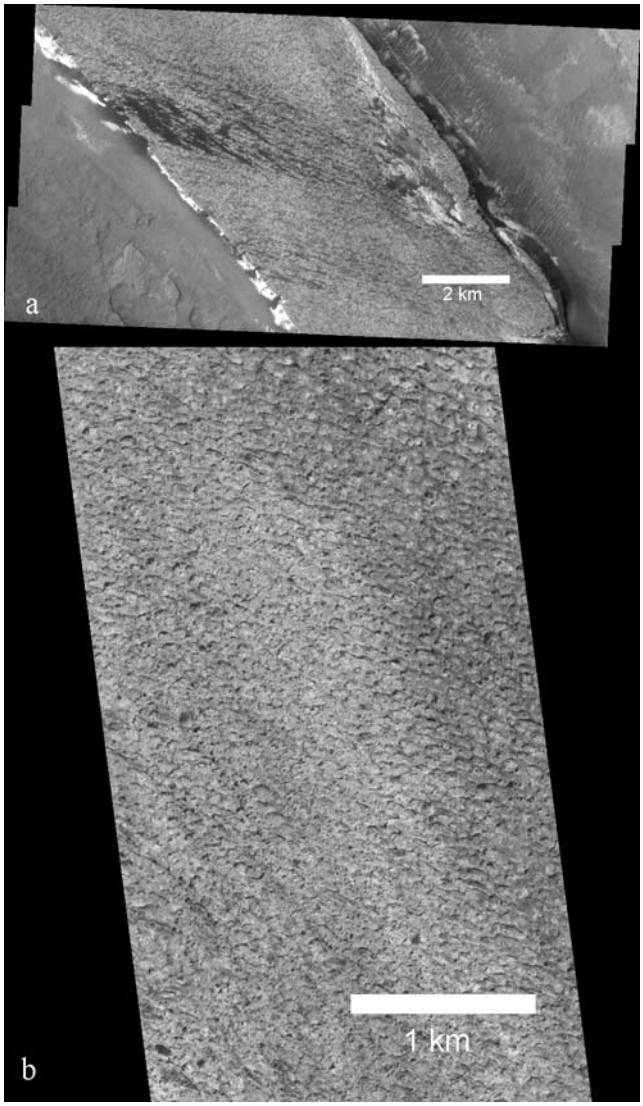

Figure 4. THEMIS and MOC images of the Cap Unit. (a) THEMIS VIS image V01511013 covering Aram Chaos Cap Unit. Dark sand is saltating across the Cap Unit and being deposited onto the terrain below. (b) Portion of MOC NA Image M2202136 covering Aram Chaos Cap Unit. This image shows a heavily fluted and pitted surface that traps dark sand.

[26] 7. The *Knobby Terrain* (C_k) unit occurs throughout the crater, often in contact with the Fractured Plains and the High Thermal Inertia Chaotic Terrain. In the north and west, this unit occurs closer to the interior of the crater than the Fractured Plains, often separating the Fractured Plains from the nondisturbed units. In the south and east, this unit often occurs as the outermost mapped unit, forming a narrow band between the Fractured Plains and the crater wall. In these regions, this unit is typically lower in elevation than the surrounding Fractured Plains. The elevation difference varies greatly, but can be up to 1 km or more. The unit is characterized by small, irregularly eroded knobs that are indicative of heavy disturbance of the original terrain. Thermal inertias within the unit range from ~350 to 410.

[27] 8. Like C_k, *High Thermal Inertia Chaotic Terrain* (C_{ht}) appears throughout the crater and is often in contact with one or both of the other chaotic terrain types. It has a higher thermal inertia than other chaotic terrains, with a range of 450–500. This unit is characterized more by fractured mounds than individual knobs, which may be indicative of either less disturbance of the original terrain or a more competent original terrain.

[28] 9. *Fractured Plains* (C_f) is the largest single unit by area in Aram Chaos. It occurs around the circumference of the crater and is characterized by large (up to tens of kilometers) slumped blocks in the south and flat plains broken by curvilinear fractures to the north and west.

[29] 10. Spectroscopic analysis of *Transported Hematite* (C_{hth}, C_{kh}) indicates the presence of small concentrations (~5%) of hematite. Unlike units P_h and P_{h2}, the hematite in these units is not associated with layered terrain. Because of the relatively low concentration, and the fact that these units are topographically below Ph, we interpret the hematite present in these units to be transported.

[30] In addition to the units described above, there is a spectral unit that was not mapped. This spectral unit is composed of basaltic sand in the northeast quadrant of the Aram Chaos crater (Figure 8). In some areas, the sand is intermixed with transported hematite, but much of the deposit is hematite-free. The sand appears to be a recent surficial unit that is not related to the formation of any of the units described above, and comparison of a decorrelation-stretched [*Gillespie et al.*, 1986] THEMIS image to a MOC wide-angle mosaic (Figure 8) shows that the distinct spectral character corresponds to dark wind-blown sand.

5. TES Spectral Analysis

5.1. Overview

[31] The derived spectral shapes of five surface units (P_c, P_h, P_s, P_{nh}, and C_f) and the basaltic sand sheet are shown in Figures 9 and 10. These units were selected for analysis based on the availability of high-quality spectra and to represent the range of features present in Aram Chaos. Results of the linear deconvolution analysis of the MGS-TES spectra representing the Aram Chaos surface units are shown in Table 2. The values are rounded to the nearest 5%. Derived modal mineralogies of the surface units fall within the stated TES detection limit of 10–15% [*Christensen et al.*, 2000b], although detailed error analysis (see below) of the surface unit spectra presented here indicates that the

Figure 3. Map and cross section of the Aram Chaos crater. (a) Map of Aram Chaos. The Aram Chaos region has been divided into 11 units based on geomorphology, thermophysical properties, and mineralogy. (b) Cross section A-B through Aram Chaos shows the stratigraphic relationships between the layered terrains and the chaotic terrain. Vertical exaggeration is 20×. The primary hematite-bearing unit is a 100–200 m deposit within the thicker stack of layered sediments. The approximate positions of the sketches in Figures 7, 12, and 13 are marked.

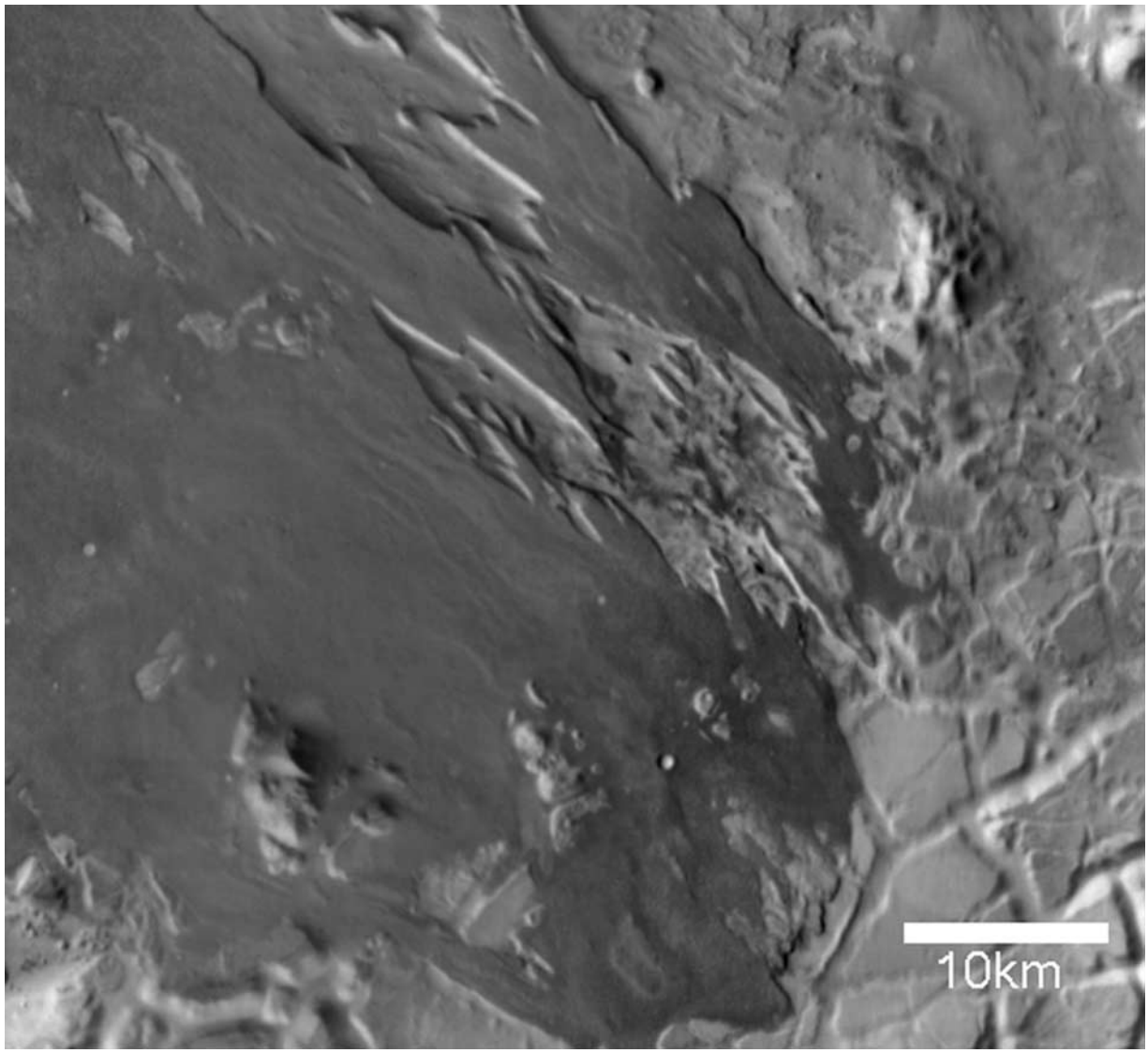

Figure 5. Close-up view of part of the infrared band 9 radiance mosaic. The southeastern part of the Cap Unit exhibits morphologies indicating that it has undergone erosion and was once more extensive.

differing spectral shapes may represent real differences in modal mineralogies at levels below the currently accepted TES detection limit.

[32] Deconvolution results of all units show an appreciable amount of carbonates present. Carbonate mineral spectra have strong absorptions near 350, 890, and 1500 cm^{-1}. As noted by *Bandfield* [2002] and *Bandfield and Smith* [2003], the deep, broad carbonate absorption at 1500 cm^{-1} is distinctive relative to silicate minerals. However, this spectral region is typically not included in the numerical deconvolutions because of difficulties in accurately removing the atmospheric components [*Bandfield et al.*, 2000; *Smith et al.*, 2000a; *Christensen et al.*, 2001b; *Bandfield and Smith*, 2003]. Following the method of *Christensen et al.* [2001b], we visibly inspected each spectrum and no carbonate feature is present above the instrument noise and atmospheric background. We conclude that carbonate abundance is significantly less than 10% and may be 0%. Although abundances of phyllosilicates and glasses are reported as a combined phyllosilicate/glass component due to the spectral similarity of the two end-member groups [*Bandfield*, 2002; *Wyatt and McSween*, 2002], glass end-members were rarely used in the deconvolution analysis. Phyllosilicate phases make up the bulk of the reported phyllosilicate/glass component. Palagonite [*Morris et al.*, 2003], zeolites [*Ruff*, 2004], and amorphous SiO_2 coatings [*Kraft et al.*, 2004] also have similar spectral characters to phyllosilicates and glass, but these phases were not used as end-members in the deconvolution.

5.2. Error Analysis

[33] Each surface spectrum shown in Figures 9 and 10 is an average of between ~50 and 100 spectra, and the dotted lines represent ±1-σ errors. Because a reliable surface atmosphere separation cannot be performed on individual spectra, an iterative approach was taken to determine the 1-σ error bars for the average surface unit

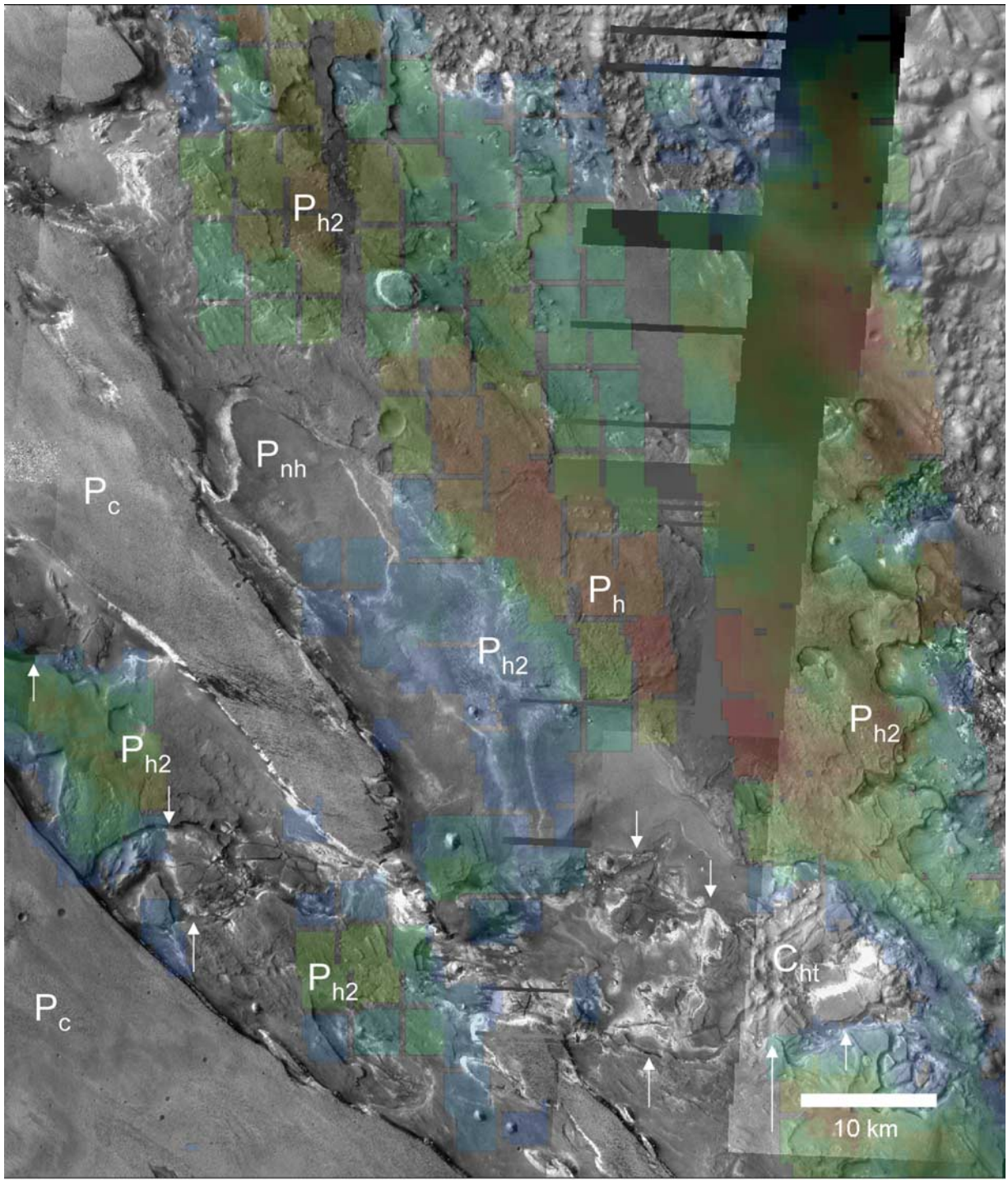

Figure 6. Hematite abundance overlaid on a THEMIS 36 m/pixel visible mosaic. The highest concentration of hematite derived from TES is confined to a relatively thin layer that has been mapped as the Primary Hematite Unit. Arrows mark the contacts between the lower layered units and the chaotic terrain lying underneath.

spectra. Individual spectra for a given surface unit were broken into groups of between 6 and 15 spectra, depending on the total number of spectra available, and averaged. The resulting "level 2" spectra were then used to determine the standard deviation. The average of the level 2 spectra was then compared to the average of all of the individual spectra to be sure that the method was valid. In all cases, the spectra being compared were nearly identical, validating the method.

5.3. Cap Unit

[34] The Cap Unit (P_c) spectral shape is not consistent with either TES Surface Type 1 (basalt) or 2 (basaltic andesite or altered/coated basalt) [*Bandfield et al.*, 2000;

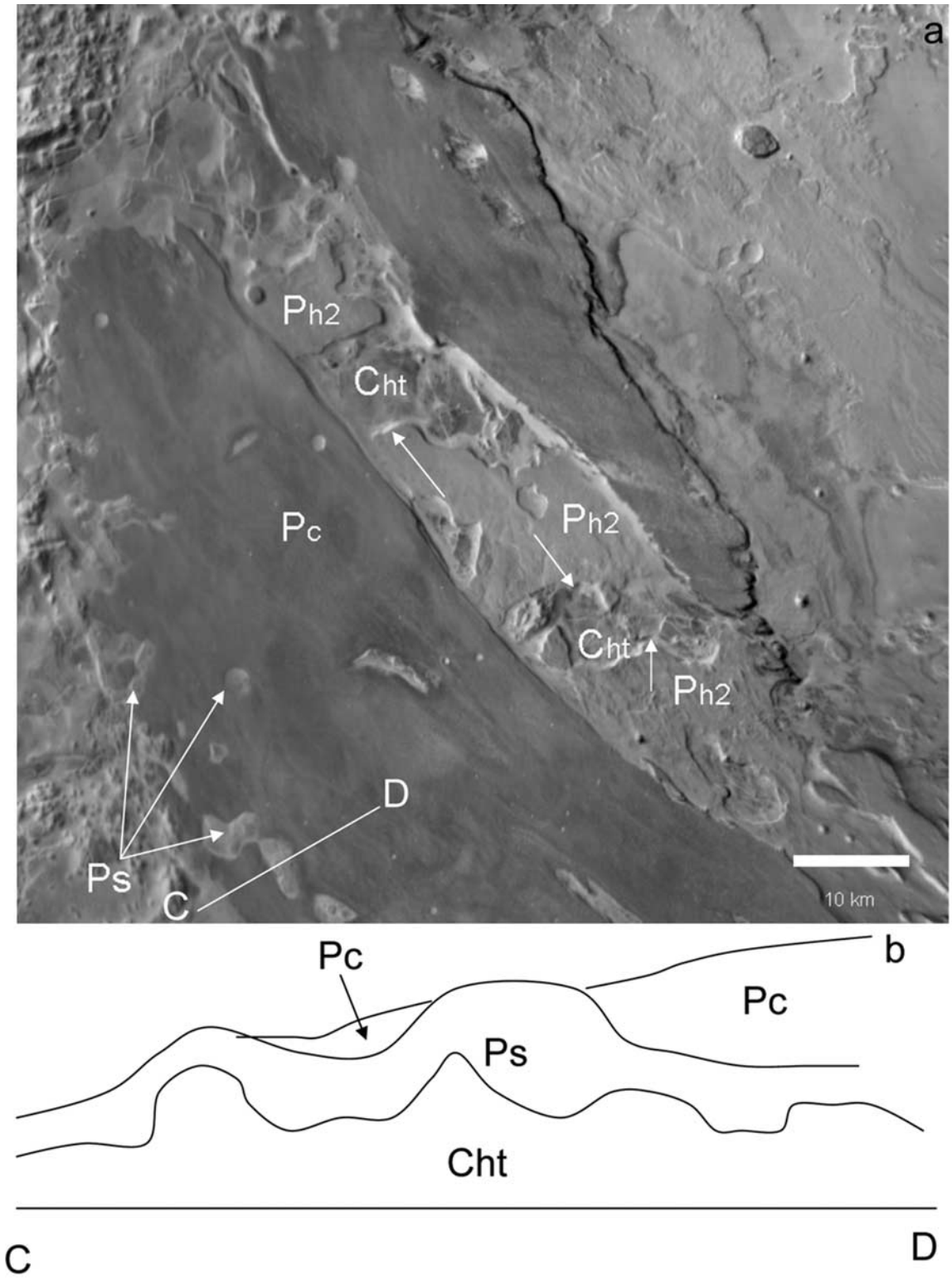

Figure 7. (a) "Window" near the center of Aram Chaos that reveals the stratigraphy of the layered units and chaotic terrain. The Cap Unit (P_c) overlies the hematite-bearing units (P_h, P_{h2}), Non-hematite Layered Terrain (P_{nh}), and Subdued Unit (P_s), which in turn overlie the chaotic terrains. Line C-D shows the location of Figure 7b. Arrows mark the position of the contact between the layered units and the chaotic terrain lying underneath. (b) Schematic cross section of the western edge of the Cap Unit, where the Subdued Unit outcrops underneath.

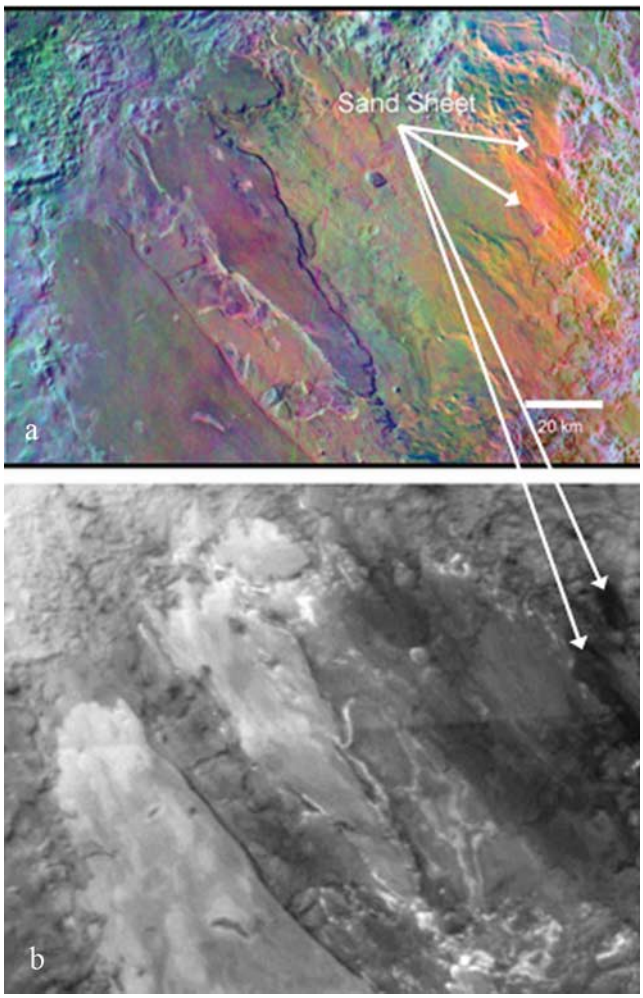

Figure 8. Distinct surficial spectral unit in Aram Chaos. (a) Decorrelation-stretch THEMIS image composed using radiance from bands 8, 7, and 5. (b) MOC wide-angle mosaic. The distinct spectral unit in the northeast of the DCS image corresponds to the surficial dark sand unit seen in the MOC wide-angle image.

Wyatt and McSween, 2002], or a mixture thereof (Figure 10), implying additional spectral component(s) are necessary to provide an accurate fit. The P_c spectrum has a low spectral contrast relative to derived global surface units [*Bandfield et al.*, 2000], with a minimum 8–12 μm emissivity of ~0.975 vs. 0.945 for the TES Surface Type 1 spectrum. The long wavelength spectral features of the P_c spectrum, however, are similar to those seen in the TES Surface Type 1 spectrum.

[35] Results of the deconvolution analysis of the average P_c spectrum indicate 10% sulfate, and 20% phyllosilicates/glass, along with 20% plagioclase feldspar and 30% pyroxene (Table 2). The phyllosilicate/glass, plagioclase, and pyroxene values are identical within the margin of error. The relatively high amount of modeled sulfate is due to the fact that the emissivity minimum for the 8–12 μm region of the P_c emissivity spectrum is at a shorter wavelength than seen in the TES Surface Type 1, the chaotic terrain, or the primarily basaltic sand sheet seen in the northeast quadrant of Aram crater (Figure 8). The spectrum also has a lower overall emissivity (compared to a scaled TES Surface Type 1 spectrum) shortward of that minimum, which is consistent with a broad sulfate absorption in that region, as well as a high pyroxene abundance.

5.4. Primary Hematite Unit

[36] The Primary Hematite unit (P_h) spectrum displays the characteristic long wavelength features of hematite [*Christensen et al.*, 2000a, 2001a; *Lane et al.*, 2002; *Glotch et al.*, 2004]. The 8–12 μm region of this spectrum differs from that of the P_c spectrum, but is still inconsistent with TES Surface Type 1 or 2 (Figure 10), or a mixture of these two spectra, again implying that additional component(s) are needed to properly fit the spectrum.

[37] Deconvolution analysis of the average P_h spectrum indicates abundances of 15% hematite, 10% sulfate, and 25% phyllosilicates/glass, along with 20% plagioclase and 15% pyroxene. These results are consistent with the results from the MiniTES experiment on the MER Opportunity Rover [*Christensen et al.*, 2004a]. The derived hematite abundance is dependent on the depth of the hematite spectral features, which vary depending on particle size. *Christensen et al.* [2001a] estimated that the maximum hematite abundance in Aram Chaos is ~15%. In this work, the contrast of the hematite spectrum was set so that the deconvolution analysis provided the estimated answer. The abundances of all other derived components scale linearly if the derived hematite abundance is increased or decreased by adjusting the spectral contrast of the hematite end-member.

5.5. Subdued Unit

[38] Like the two previously described units, the Subdued Unit (P_s) is not consistent with either TES Surface Type 1 or 2, or a mixture thereof (Figure 10). Like the P_c spectrum, the P_s spectrum has low spectral contrast, with a minimum 8–12 μm emissivity of ~0.977. As is seen when the P_c and the P_h spectra are deconvolved, analysis of the average P_s spectrum results in relatively high abundances of sulfate (10%) and phyllosilicate/glass (20%). Abundances of plagioclase (30%) and pyroxene (25%) are consistent with a sedimentary unit derived from a primarily igneous rock with the addition of sulfate and phyllosilicates/glass as cements or other components.

5.6. Non-Hematite Layered Terrain

[39] The spectral shape of the Non-Hematite Layered Terrain (P_{nh}) unit in eastern Aram Chaos is similar to that of P_s (Figure 10). It also has a similar spectral contrast, with a minimum 8–12 μm emissivity of 0.975. Results from the deconvolution of the average P_{nh} spectrum are similar to the results from P_s, with comparable amounts of plagioclase, pyroxene, sulfate, and phyllosilicate/glass (Table 2).

5.7. Chaotic Terrain/Dark Sand

[40] Two spectral units within Aram Chaos can be well modeled as combinations of the TES Surface Type 1 and 2 spectra. The chaotic terrains, which include Fractured Plains (C_f), Knobby Terrain (C_k), and High Thermal Inertia Chaotic Terrain (C_{ht}), have similar spectra that resemble the TES Surface Type 1 spectrum. An example Fractured

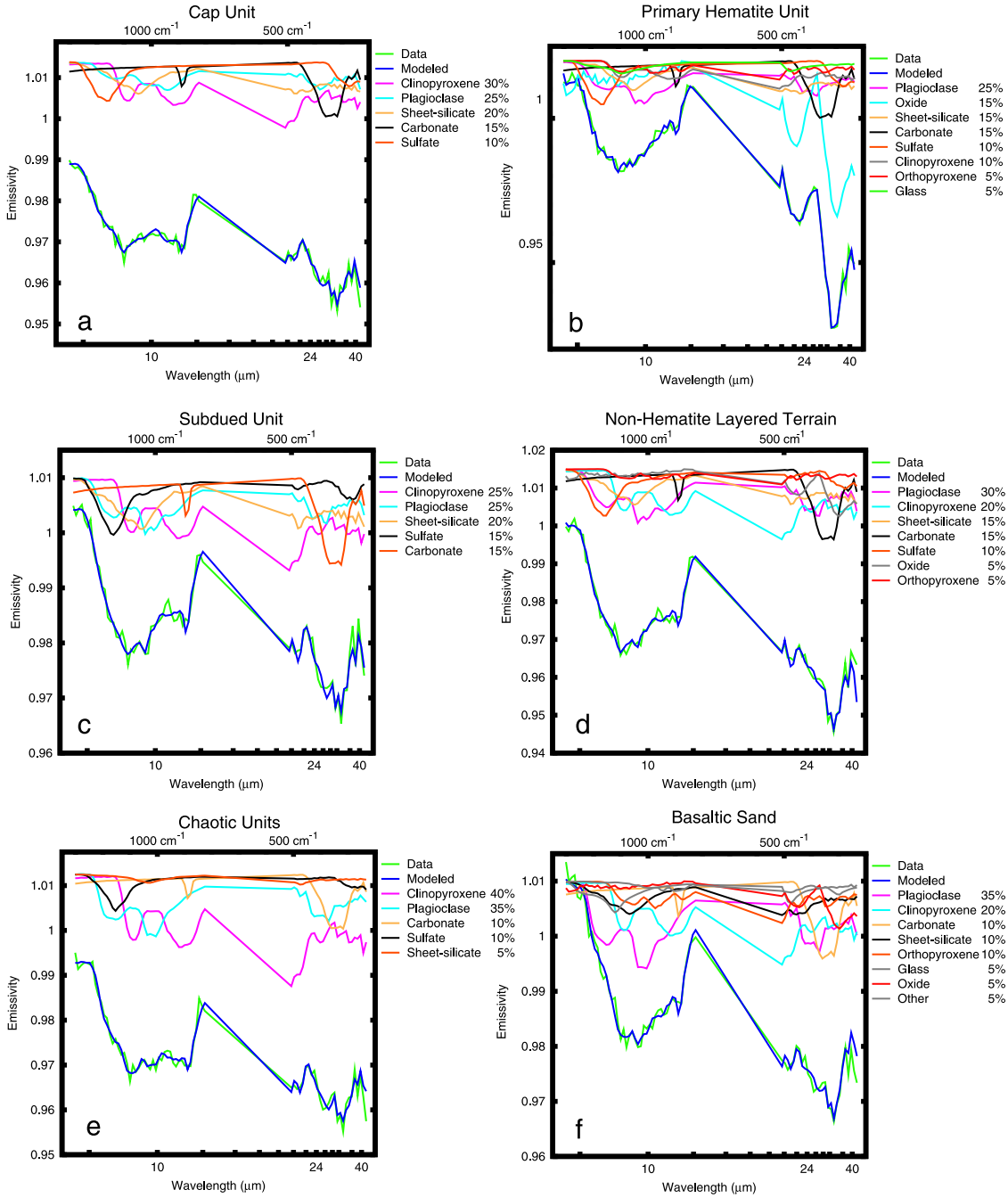

Figure 9. MGS-TES spectra of the mapped surface units, and the modeled best fits using Library 2 (Table 1). The surface spectrum, the modeled best fit, and the spectra of the components used, scaled to their modeled abundances, are shown. (a) Cap Unit, (b) Primary Hematite Unit, (c) Subdued Unit, (d) Non-Hematite Layered Terrain, (e) Fractured Plains, and (f) Basaltic Sand Sheet.

Plains spectrum is shown in Figure 10. The match to TES Surface Type 1 is particularly good at long wavelengths, and the 8–12 μm region has the typical shape of the TES Surface Type 1 spectrum, although the 11–12 μm region has a somewhat lower emissivity than is seen in a scaled TES Surface Type 1 spectrum. The sand sheet in the northeast portion of Aram Chaos (Figure 8) has a spectrum that can be modeled well as ~65% TES Surface Type 1 and ~35% TES Surface Type 2. In contrast to the layered units, significant amounts of sulfate are not modeled for either this unit or the chaotic terrain, and the chaotic terrain also appears to be relatively free of phyllosilicate/glass phases.

6. Discussion

6.1. Stratigraphic Relationships

[41] The stratigraphic relationships between the units provide significant insights for determining the geologic history of Aram Chaos, especially the timing between the formation of the interior layered deposits and the chaotic

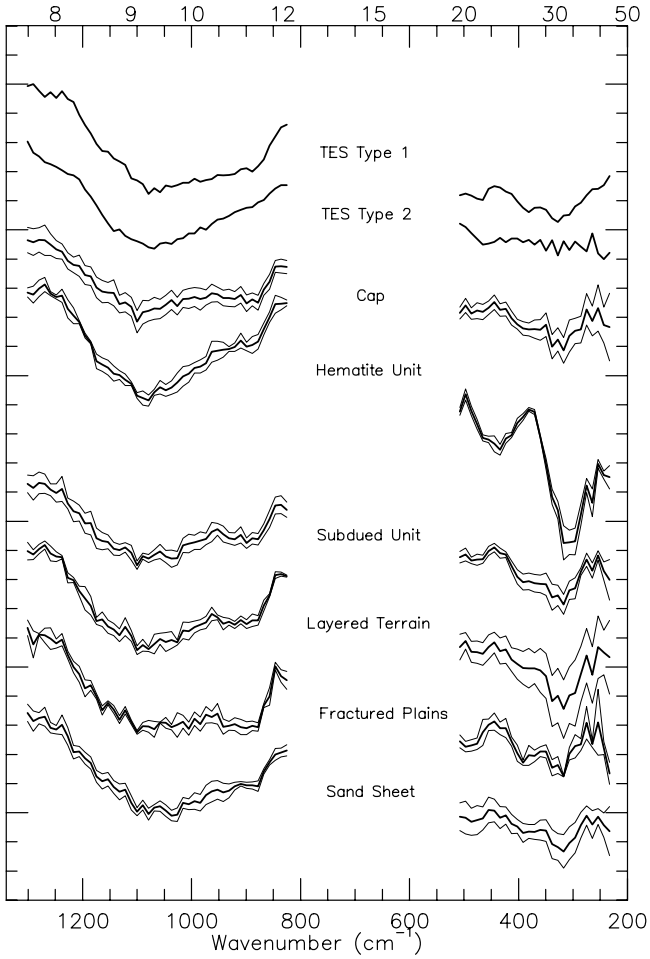

Figure 10. MGS-TES spectra of the Aram Chaos surface units compared to TES global surface units. The Cap Unit is the most spectrally unique and cannot be modeled as a combination of TES Types 1 and 2. Spectra of the Subdued Terrain, Layered Terrain, and Primary Hematite Unit exhibit similar spectral features between 8 and 12 μm. Spectra of the Fractured Plains and the Sand Sheet are close to TES Surface Type 1.

terrain units. In at least three locations (Figure 11), outliers of the Cap unit (P_c) can be seen infilling fractures of the chaotic terrains. Therefore P_c (the topmost stratigraphic unit of the interior layered deposits) and the layered units below it appear to have been deposited after the initial formation of the chaotic units (Fractured Plains (C_f), High Thermal Inertia Chaotic Terrain (C_{ht}), and Knobby Terrain (C_k)). It is unlikely that the regions shown in Figure 11 are a result of material eroding off of P_c and filling the fractures. There are no aeolian bedforms present in these areas. In fact, the outlier units appear to erode similarly to the main deposit. The outlier material is thermophysically identical to the main outcrops of P_c, indicating that the fracture-filling material is composed of loose sediments.

[42] Near the center of the crater, there is a window (Figures 7 and 12) through the layered units where portions of disrupted chaotic terrain (C_{ht}) can be seen underneath interior layered deposits. In this area, disturbed material (chaotic terrain) occurs directly below a large deposit of eroded, undisturbed layered material. The direct superposition of undisturbed material on disturbed terrain is further evidence that the interior layered deposits must have been deposited subsequent to the formation of at least unit C_{ht}.

[43] To the west of the main interior layered deposit, Subdued Terrain (P_s) outcrops directly below P_c (Figure 7). Because P_s lies stratigraphically directly below P_c, we interpret this unit to represent a lateral facies change within P_h, which also lies stratigraphically directly below P_c in the east. This relationship is expressed in the cross section in Figure 3, and the interpretation is strengthened by TES data, which show that P_s and P_h have similar mineral compositions other than hematite abundance (Table 2). We suggest that the depositional basin was shallower in the western part of Aram crater, with a pinching out of the last sedimentary unit deposited before P_c. The muted appearance of knobs and chaotic fractures within P_s gives the impression that this unit is a relatively thin layer overlying Knobby terrain (C_k).

[44] In Figure 3, only about 20% of the hematite-rich terrain was mapped as the Primary Hematite unit (P_h). This unit conforms to a distinct region best seen in the THEMIS visible imagery (Figure 6). This unit lies stratigraphically above the other layered terrains that contain lower concentrations of hematite. We agree with the interpretation of *Catling and Moore* [2003] that much of the hematite is present as a lag deposit, although aeolian transport of hematite may also have occurred.

6.2. Nature of Layered Terrains and the Occurrence of Sulfate

[45] The four types of layered terrain (Cap unit (P_c), Hematite units(P_h and P_{h2}), Subdued unit (Ps), and Non-Hematite Layered Terrain (P_{nh})) show a systematically higher concentration of sulfates than is seen in either the chaotic terrain, or in the primarily basaltic sand sheet (Figure 8) present in the northeast portion of Aram Chaos. The relative difference in sulfate abundance between the layered terrains and other units within Aram Chaos suggests that sulfates are present and variable within these units. Based on laboratory work and analysis of TES data, *Cooper and Mustard* [2001, 2002] suggested that sulfate-rich duricrusts may be present on Mars. MiniTES data from the surface at Meridiani Planum have identified Ca and Mg sulfates in light-toned rock outcrops [*Christensen et al.*, 2004a]. The occurrence of hematite at Meridiani Planum and Aram Chaos, the detection of sulfates at Meridiani with MiniTES, and the identification of sulfates at the 10% level in Aram Chaos with TES data suggests that similar environments may have existed at Meridiani Planum and Aram Chaos, which were compatible with the formation of sulfate minerals.

[46] *Baldridge and Calvin* [2004] showed that spectra collected by Mariner 6 and 7 over Meridiani Planum and Aram Chaos had an increased 3 μm band depth, indicative of hydrated minerals. They hypothesized that the increased 3 μm band depth was due to the presence of some hydrous phase or phases associated with the hematite. Kieserite and other hydrated minerals associated with the hematite deposit were also identified with the European Space Agency's OMEGA near infrared spectrometer [*Gendrin et al.*, 2005].

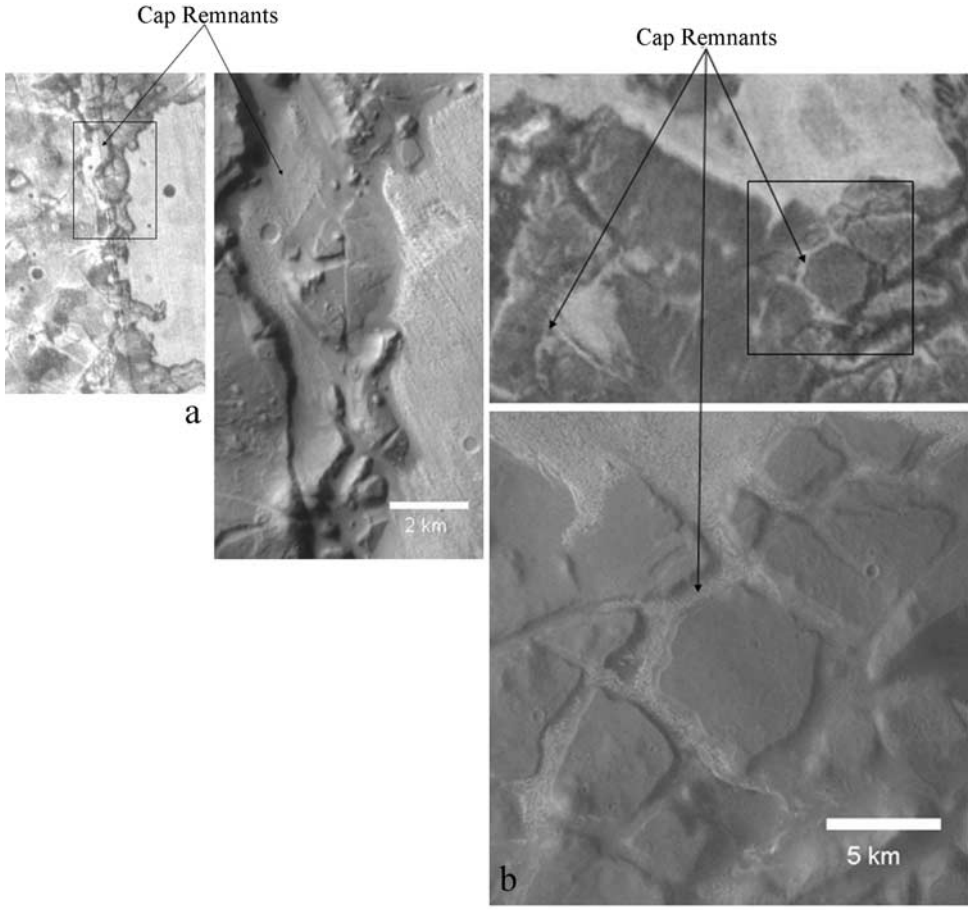

Figure 11. Remnants of the Cap Unit infill fractures of the chaotic terrain. (a) THEMIS nighttime infrared and visible imagery of the northwest portion of the Cap Unit, where cap material is infilling a small fracture of the High Thermal Inertia Chaotic Terrain. (b) THEMIS nighttime infrared and visible imagery of the southeast portion of the Cap Unit where cap material is infilling fractures in the Fractured Plains unit.

There are many sulfate species that contain abundant water in their structures, including but not limited to, gypsum ($CaSO_4 \cdot 2H_2O$), bassanite ($CaSO_4 \cdot 1/2\ H_2O$), kieserite ($MgSO_4 \cdot H_2O$), and epsomite ($MgSO_4 \cdot 7H_2O$). Additionally, each of the layered units has a modeled glass/phyllosilicate abundance of 20–25%, and water could also be present in these phases.

[47] The similarities in TES spectra, albedo, and thermal inertia between P_s and P_{nh} indicate that they could be related. These relationships suggest that P_s and P_{nh} formed

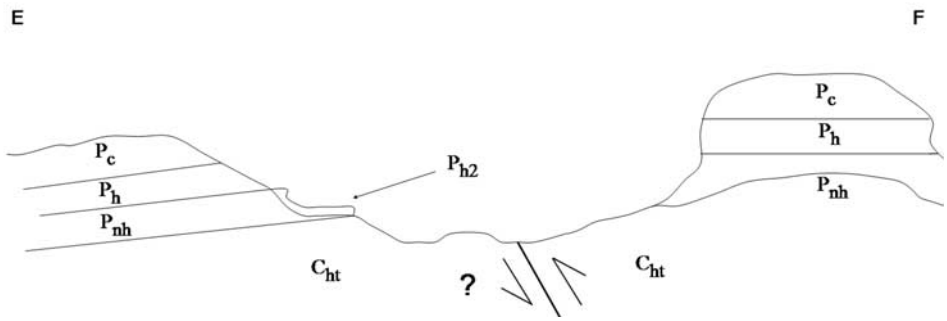

Figure 12. Sketch of the window near the center of Aram Chaos (line E-F in Figure 3a). Chaotic terrain is exposed through the eroded layered section, and hematite eroded from Ph is deposited as an alluvial layer on top Non-Hematite Layered Terrain. The offset in the elevation of the Cap Unit and the inferred position of the Primary Hematite Unit suggests that the layers are tilted and/or separated by a normal fault.

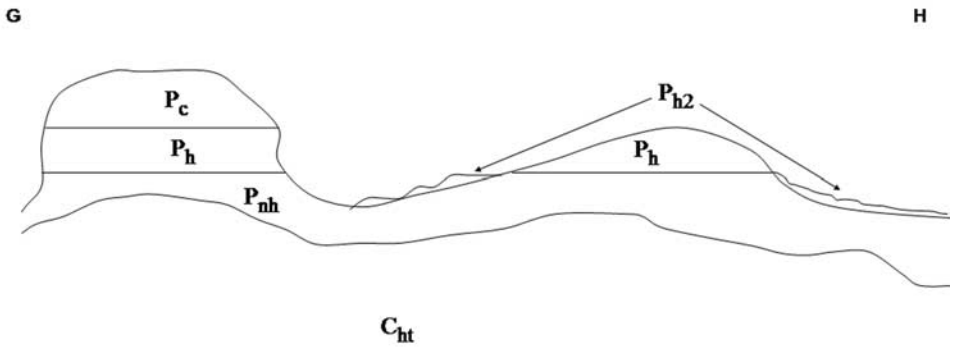

Figure 13. Sketch of the stratigraphic relationships in northeastern Aram Chaos (Line G-H in Figure 3a). The Primary Hematite Unit (P_h) is confined to a single ~100 m thick layer, and is stratigraphically directly below the Cap Unit (P_c). Hematite is transported from P_h downslope and is present at lower concentrations on top of the Non-Hematite Layered Unit (P_{nh}).

under similar conditions and by similar processes. It is unlikely that the two units were deposited at the same time, though. P_s outcrops directly below P_c in western Aram Chaos. In eastern Aram Chaos, the unit that is stratigraphically directly below P_c is P_h (Figure 13). This relationship may be indicative of a horizontal facies change in the unit directly below P_c.

[48] Among the undisturbed layered units within Aram Chaos P_c is unique. This unit has a distinct combination of properties (higher albedo than the surrounding units (0.165–0.18 versus 0.12–0.14), higher thermal inertia, and lower spectral contrast) that characterize it. The intrinsic albedo of the cap material is likely even higher than that recorded by TES, as within any given TES pixel, there will be a mixture of cap material and dark sand. A similar effect is seen at White Rock, where the intrinsic albedo of the White Rock deposits was shown to be higher than that measured by MGS-TES, due to the mixture of dark sand with the White Rock deposits [*Ruff et al.*, 2001].

[49] As stated earlier, given the thermal inertia of P_c (~400–500), it is most likely less disaggregated with larger clasts than the other layered units. The relatively high amount of modeled sulfate could serve as a cementing agent for the basaltic sediments that compose most of P_c, but it is not clear what effect a sulfate cement would have on the spectral contrast of the P_c TES spectrum. Other materials that commonly form cements, such as halides, have no deep features in the mid-IR [*Baldridge*, 2002], and may effectively reduce the spectral contrast of the matrix material.

6.3. Chaotic Terrain

[50] Three distinct forms of chaotic terrain have been observed in Aram Chaos. We interpret these three units as the result of three different degrees of disturbance of the original terrain in Aram Crater. From least disturbed to most disturbed, these units are C_f, C_{ht}, and C_k. These terrain types represent either lateral variation in the prechaotic terrain competence, lateral variation in subsurface water content, or a temporal variation in chaos-forming processes. These terrains are distinct in terms of morphology and mineralogy from the interior layered deposits, and superposition relationships show that they existed within Aram Crater before the interior layered units were deposited.

7. Lacustrine Model for the Formation of Aram Chaos

[51] The observations and interpretations of the units within Aram Chaos can be explained by a lacustrine model for their formation. The interpretation of Aram Chaos as a lacustrine environment is dependent on six key observations: (1) The presence of interior layered deposits, (2) the occurrence of gray hematite within this layered sequence of rocks, (3) the fact that the layered units lie within a closed basin, (4) the existence of chaotic terrain and an outflow channel, indicating the presence of extensive subsurface ice or water, (5) the observation that the layered deposits were emplaced subsequent to the formation of the chaotic terrain, and (6) the poor match between the thermal infrared spectra of magnetite-derived hematites and the Martian hematite [*Glotch et al.*, 2004]. The first five observations alone, while providing strong circumstantial evidence for the formation of hematite in a water-rich environment, do not rule out a volcanic origin for the deposits. They are also consistent with the deposition of a magnetite-rich ash layer subsequent to the formation of the chaotic terrain, and later alteration of magnetite to hematite. However, *Glotch et al.* [2004] showed that magnetite-derived hematite is a poor mid-IR spectral match to the Martian hematite. Rather, hematite samples that were formed at low temperature and exhibited disorder in the hematite cation framework structure proved to be good spectral matches to the Martian hematite. It is this spectroscopic observation that makes a magnetite pathway for the formation of the Martian hematite unlikely.

[52] Similar to Meridiani Planum, it is possible that the hematite at Aram Chaos formed by a secondary diagenetic process involving the dissolution of the sulfate-rich outcrop rock. However, the easiest way to reconcile all of the observations is a model in which the layered units are deposited in a lacustrine environment that existed subsequent to the formation of the chaotic terrains, and the hematite formed via a late-stage diagenetic process. A likely

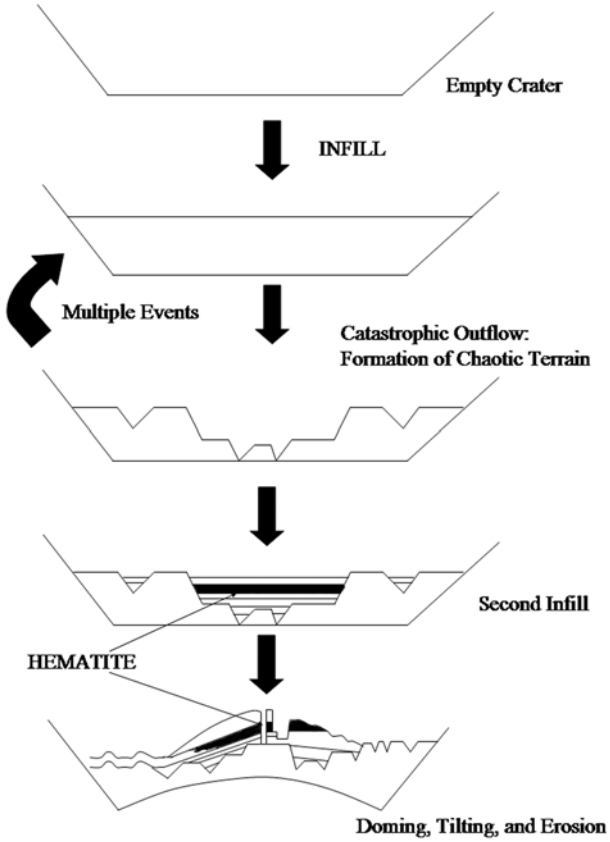

Figure 14. Schematic representation of the chain of events leading to the current state of Aram Chaos in the lacustrine model. An empty crater is filled with material and a subsurface aquifer breaks through, leading to the formation of the chaotic terrain. Multiple catastrophic floods, followed by ponding lead to the formation of layered terrains (one of which contains hematite) above the chaotic terrain. Subsequent tilting and erosion are responsible for Aram Chaos in its current state.

model is shown in Figure 14. An empty impact crater is filled with sediment, perhaps by aeolian deposition. There is ample evidence for the infilling of other nearby craters with sediment [*Malin*, 1976; *Christensen et al.*, 2001a; *Edgett and Malin*, 2002]. Catastrophic release of a subsurface aquifer leads to the formation of the chaotic terrain, and before the water flows out of the channel, it ponds, and layered sediments are deposited. Release of the aquifer, ponding of water, and deposition of layered sediments may have occurred multiple times. Only a single layer within the sequence of sediments contains hematite, so we hypothesize that this layer was deposited with a "seed" of extra iron, perhaps in the form of a pulse of hydrothermal fluid. Alternatively, it may be that only a single layer was permeable enough to allow the passage of diagenetic fluids [*Ormö et al.*, 2004]. In either case, if the entire layered sequence was exposed to diagenetic conditions, then this layer would preferentially form hematite. It is also possible that the layered materials were reworked by aeolian activity, but their sulfate and glass/phyllosilicate-rich nature is indicative of deposition in a water-rich environment.

[53] Over time, a dome-shaped structure (Figure 15) near the center of the crater formed, leading to tilting of the layered units, and erosion of the layered units exposed the chaotic terrain underneath. If the hematite in Aram Chaos was originally deposited as goethite or some other iron oxyhydroxide, as suggested by *Glotch et al.* [2004], then it is possible that geothermal heat associated with a deformation event that formed the dome structure in the center of the crater (Figure 15) could have been responsible for the formation of hematite from the precursor mineral. Two specific complexities of this model are discussed below.

8. Model Complexities

8.1. Formation of Chaotic Terrain

[54] Episodic pulses of water release have been judged to be likely in the formation of chaotic terrain and outflow channels [*Baker et al.*, 1991]. Recent modeling of pressurized aquifers within the Martian regolith showed that multiple flooding events from a chaos region are likely due to the slow diffusion of pressure waves within aquifers [*Hanna and Phillips*, 2003]. This type of model may explain the formation of the three types of Aram Chaos chaotic units. The first release of subsurface water formed unit C_f throughout the crater. A second release, some time later, affected a smaller area of Aram, and reworked some of the dissected plains, creating C_{ht}. A third (and possibly subsequent pulses) further reworked the chaotic materials within the crater, forming C_k. It is likely that further pulses of water were responsible for the deposition of the layered terrains. A single, large event would probably have created

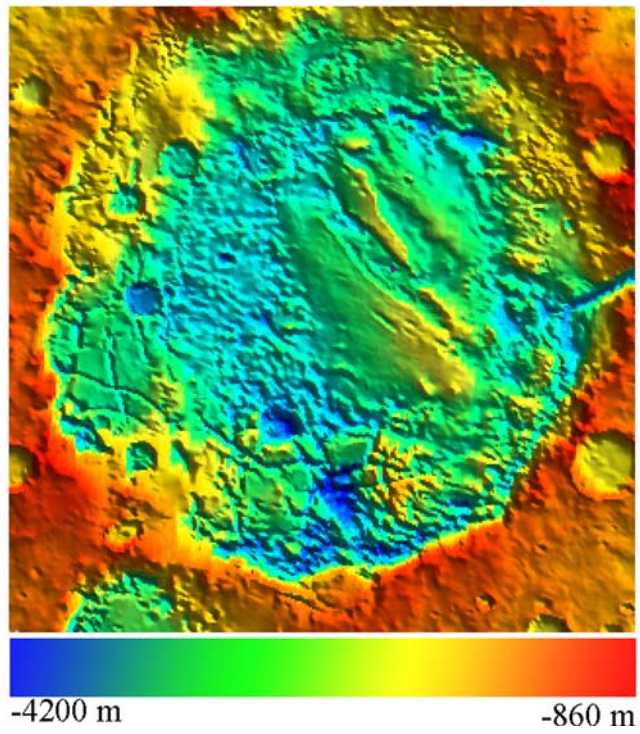

Figure 15. MOLA topography illustrating the dome-shaped structure in east central Aram Chaos.

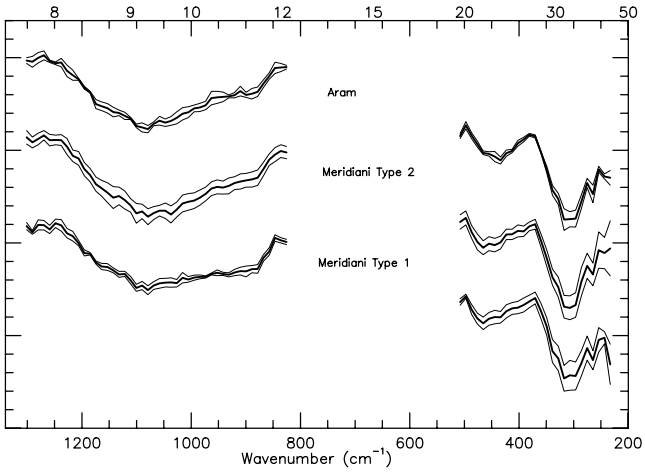

Figure 16. Comparison of representative spectra from the Aram Chaos and Meridiani Planum hematite units. The Meridiani Planum hematite unit exhibits the spectral character of hematite plus TES Surface Type 1, and hematite plus TES surface Type 2, which is more similar to the Aram Chaos spectrum.

one massive, non-layered unit stratigraphically above the chaotic terrains.

8.2. Postdepositional Deformation

[55] MOLA data (Figures 3 and 15) show a broad, dome-shaped structure near the center of Aram Chaos. P_c covers the broad western slope of the dome for ~700 m of vertical relief. However, profiles over the window at the center of the crater show that, at least in this area, unit P_c is ~200 m thick. While it is likely that erosion contributed to the current topography, no erosional processes can account for the combination of (1) the 700 m total relief of the western part of the dome, (2) the observed 200 m thickness of P_c near the top of the dome, and (3) the observed thinning of P_c to the west as evidenced by the appearance of Ps from underneath Pc (Figure 7). The layered units must have been tilted to account for these observations. Comparison of elevations of C_{ht} in the window at the center of the crater (Figures 7 and 12) and of the same unit in the western part of the crater, show an average 200 m elevation difference, which translates to a slope of 0.3° to the west. It is possible that subsequent to the deposition of the layered units, Aram Chaos experienced regional tectonic activity for some time, including the formation of an extensional fault near the center of the crater (Figure 3). This would be consistent with an interpretation of the window through the layered units (Figures 7 and 12) as a graben. Uplift caused by volcanic intrusion would be consistent with some hypotheses regarding the formation of chaotic terrains [*Maxwell and Picard*, 1974; *Masursky et al.*, 1977]. This type of activity may have tilted the layered beds, and caused the dome-shaped structure seen near the center of Aram Chaos.

9. Relationship Between Aram Chaos and Meridiani Planum

[56] There is a strong similarity between the layered units seen in Aram Chaos and Meridiani Planum in terms of thickness and thermal inertia. As is seen in Meridiani Planum, the source of the hematite is a thin layer within a much thicker stack of sediments [*Christensen et al.*, 2000a, 2001a; *Hynek et al.*, 2002]. Hematite is also seen in non-layered material (Knobby Terrain and High Thermal Inertia Chaotic Terrain) in the eastern portion of Aram Chaos. These areas were interpreted as lag deposits by *Catling and Moore* [2003]. This may be the case, although we note that it is possible that hematite-bearing material may have been transported by wind to the chaotic terrain.

[57] The science results from the MER Opportunity rover [*Squyres et al.*, 2004; *Christensen et al.*, 2004a; *Klingelhöfer et al.*, 2003] and analysis of TES, THEMIS, and MOLA data over Meridiani Planum [*Christensen and Ruff*, 2004], provide context for the discussion of hematite mineralization in Aram Chaos. The hematite unit in Meridiani Planum lies within a topographic trough over 75% of its circumference and the remaining perimeter is <150 m lower in elevation [*Christensen and Ruff*, 2004], implying that the hematite-bearing deposits may have formed in a basin. The hematite unit within Aram Chaos was deposited in an obvious basin. This similarity may be circumstantial, or it may point to a preferred mechanism for gray hematite formation on Mars. Additionally, the hematite in Meridiani Planum has been shown to occur as ~3–5 mm concretions [*Soderblom et al.*, 2004] that weather out of a sulfate-rich outcrop. The possible detection of sulfate within the layered units in Aram Chaos also points to a common formation mechanism for hematite between Aram Chaos and Meridiani Planum.

[58] There are, however, several differences between Aram Chaos and Meridiani Planum that must be considered when comparing the regions. This study has shown that the hematite in Aram Chaos does not occur in a substrate that can be accurately modeled as either TES Surface Type 1 or TES Surface Type 2. While the hematite in Meridiani Planum occurs primarily in a basaltic substrate [*Christensen et al.*, 2000a, 2001a; *Christensen and Ruff*, 2004], investigation of TES spectra over Meridiani Planum also shows spectra that are consistent with the Aram Chaos hematite unit spectrum. A comparison of typical Meridiani Planum and Aram Chaos hematite unit spectra is shown in Figure 16, and the derived modal mineralogy for each unit is shown in Table 3. Relatively higher (although not statistically significant) abundances of phyllosilicates and sulfate are modeled in the deconvolution of the Aram Chaos P_h unit relative to the two typical Meridiani Planum spectra. Additionally, both Meridiani units have a statistically significant higher amount of plagioclase feldspar. Although there appear to be differences in the long wavelength portion of the spectra,

Table 3. Derived Surface Mineralogies of Aram and Meridiani Hematite Units

Component	Aram Hematite	Meridiani Type 1	Meridiani Type 2
Plagioclase	20	30	30
Pyroxene	15	25	20
Hematite	15	15	15
Sulfate	10	5	5
Carbonate	15	10	10
Glass/Phyllosilicate	30	20	20

this is most likely due to the convolution of the hematite, pyroxene, and feldspar spectral features at these wavelengths. The hematite components of the spectra, as determined by factor analysis and target transformation are virtually identical [*Glotch et al.*, 2004]. The differences seen between the Meridiani Planum and Aram Chaos hematite-bearing units may be due simply to the composition of the surrounding terrain, or they may point to different processes forming the layered units within Meridiani Planum and Aram Chaos.

[59] *Christensen and Ruff* [2004] show that the hematite-bearing unit in Meridiani Planum is thermophysically distinct from the surrounding plains material. The TES-derived thermal inertia of unit Ph in Meridiani Planum is ~170–240 [*Christensen and Ruff*, 2004], versus a value of ~280–315 for unit P_h in Aram Chaos. The other layered terrains (excluding P_c) in Aram Chaos have derived thermal inertias as high as 350. Unit P_c is distinct, with derived thermal inertia ranging from ~400–500. There is no comparable high thermal inertia unit that lies stratigraphically above unit Ph in Meridiani Planum.

[60] There appears to be a significant difference in age between the events that formed the hematite-bearing units in Aram Chaos and Meridiani Planum. Crater counts over Meridiani Planum [*Lane et al.*, 2001, 2003; *Hartmann et al.*, 2001] suggest that the region has undergone an extensive burial and exhumation process. *Hynek et al.* [2002] put an upper limit on the age of the hematite-bearing unit in Meridiani Planum at 3.7 Ga, although *Lane et al.* [2003] propose and age closer to 4 Ga based on counts of eroded "fossil" craters. By contrast, Aram Chaos appears to be substantially younger. Crater counts and detailed geologic mapping [*Rotto and Tanaka*, 1995; *Tanaka et al.*, 2003; *Tanaka and Skinner*, 2004] have placed the formation of Aram Chaos in the Late Hesperian (~3 Ga [*Hartmann and Neukum*, 2001]). Therefore the absolute age difference between the events that formed the hematite-bearing plains in Aram Chaos and Meridiani Planum is ~0.7–1.0 Gyr. The large gap in time (as well as distance) between the formation of hematite at Aram Chaos and Meridiani Planum certainly points to separate events, if not necessarily separate hematite formation processes.

[61] The possible formation of a lake in Aram Chaos at ~3 Ga represents an event that is significantly younger than the proposed clement period on Mars [*Pollack et al.*, 1987; *Pepin*, 1994; *Jakosky and Phillips*, 2001]. If a proposed northern ocean formed as a result of outflow channel activity [*Parker et al.*, 1989, 1993], then a lake in Aram Chaos may have been present coincident with this ocean. A lake in Aram Chaos may have predated or postdated a proposed northern ocean depending on whether the formation of the ocean was coincident with the Chryse outflow channels [*Parker et al.*, 1989, 1993] or if it was present before the formation of the outflow channels [*Edgett and Parker*, 1997; *Baker et al.*, 1991; *Head et al.*, 1991].

10. Conclusions

[62] Analysis TES, THEMIS, MOLA, and MOC data sets over the Aram Chaos region of Mars has resulted in the following conclusions.

[63] 1. Large volumes of water were released during the formation of the chaotic terrain, as evidenced by the 15 km wide outflow channel that intersects Ares Valles.

[64] 2. In at least three areas in Aram Chaos, remnants of the Cap unit directly infill fractures within the chaotic terrains. This observation, in addition to the stratigraphy displayed in the window near the center of Aram Chaos supports the hypothesis that the layered units in Aram Chaos were deposited after the formation of the chaotic terrains.

[65] 3. TES spectra of the layered units within Aram Chaos indicate elevated abundances of glass/phyllosilicate and sulfates compared to the chaotic terrains and a basaltic sand sheet in the northeast quadrant of the crater. The layered unit stratigraphically below the Cap Unit contains gray, crystalline hematite.

[66] 4. These observations, taken with fact that the Aram Chaos hematite is a poor spectral match to magnetite-derived (i.e., volcanically derived) hematite, and the obvious basin morphology of Aram Chaos, point to subaqueous deposition of the layered units.

[67] 5. If the hematite in Aram Chaos was originally deposited as goethite or another iron oxyhydroxide, then an increased geotherm associated with postdepositional deformation in the crater is a possible explanation for the conversion of the precursor mineral to hematite.

[68] 6. There are many similarities between the hematite-bearing units in Aram Chaos and Meridiani Planum, although the hematite-forming events may have been separated by as much as 1 Gyr. If the hematite-bearing units in Meridiani Planum and Aram Chaos both formed as a result of subaqueous deposition, then the Martian atmosphere may have been significantly thicker in the Hesperian than previously thought. Alternatively, the episodic catastrophic release of volatiles may have temporarily created an environment in which the hematite-bearing deposits were laid down in a similar manner as those seen in Meridiani Planum.

[69] **Acknowledgments.** We would like to thank Wendy Calvin and Goro Komatsu for detailed reviews that significantly improved the content and clarity of the manuscript. We would also like to thank Deanne Rogers and Joshua Bandfield for thoughtful reviews and discussions of an early version of the manuscript. Thanks to Kelly Bender, Laurel Cherednik, Kim Murray, Kim Homan, Noel Gorelick, Sadaat Anwar, and Greg Mehall at Arizona State University for their planning, acquisition, processing, and software support of the TES and THEMIS data. Additional thanks to Mike Wyatt and Trent Hare for their assistance with GIS issues and to Christopher Edwards and Ben Steinberg for their assistance in creating THEMIS mosaics.

References

Arvidson, R. E., F. P. Seelos IV, K. S. Deal, W. C. Koeppen, N. O. Snider, J. M. Kieniewicz, B. M. Hynek, M. T. Mellon, and J. B. Garvin (2003), Mantled and exhumed terrains in Terra Meridiani, Mars, *J. Geophys. Res.*, *108*(E10), 8073, doi:10.1029/2002JE001982.

Baker, V. R., R. G. Strom, V. C. Gulick, J. S. Kargel, G. Komatsu, and V. S. Kale (1991), Ancient oceans, ice sheets and the hydrological cycle on Mars, *Nature*, *352*, 589–594.

Baldridge, A. (2002), Mars remote sensing analog studies in Badwater Basin, Death Valley, CA: Groundtruth and analysis of surface samples, Masters thesis, Ariz. State Univ., Tempe.

Baldridge, A. M., and W. M. Calvin (2004), Hydration state of the Martian coarse-grained hematite exposures: Implications for their origin and evolution, *J. Geophys. Res.*, *109*, E04S90, doi:10.1029/2003JE002066.

Bandfield, J. L. (2002), Global mineral distributions on Mars, *J. Geophys. Res.*, *107*(E6), 5042, doi:10.1029/2001JE001510.

Bandfield, J. L., and M. D. Smith (2003), Multiple emission angle surface-atmosphere separations of Thermal Emission Spectrometer data, *Icarus*, *161*, 47–65.

Bandfield, J. L., V. E. Hamilton, and P. R. Christensen (2000), A global view of Martian surface compositions from MGS-TES, *Science*, *287*, 1626–1630.

Bandfield, J. L., D. Rogers, M. D. Smith, and P. R. Christensen (2004), Atmospheric correction and surface spectral unit mapping using Thermal Emission Imaging System data, *J. Geophys. Res.*, *109*, E10008, doi:10.1029/2004JE002289.

Barron, V., J. Torrent, J. P. Greenwood, and R. E. Blake (2004), Can the phosphate sorption and occlusion properties help to elucidate the genesis of specular hematite on the mars surface? [CD-ROM], *Lunar Planet. Sci.*, *XXXV*, abstract 1853.

Bell, J. F., III, et al. (2004), Pancam multispectral imaging results from the Opportunity rover at Meridiani Planum, *Science*, *306*, 1703–1709.

Berner, R. A. (1969), Goethite stability and the origin of red beds, *Geochim. Cosmochim. Acta*, *33*, 267–273.

Brown, J. B. (1971), Jarosite-Goethite stabilities at 25°C, 1 ATM, *Mineral. Deposita*, *6*, 245–252.

Calvin, W. M., A. Fallacaro, and A. Baldridge (2003), Water and hematite: On the spectral properties and possible origins of Aram, Meridiani, and Candor, paper presented at Sixth International Conference on Mars, abstract 3075, Lunar and Planet. Inst., Pasadena, Calif.

Carr, M. H. (1979), Formation of Martian flood features by release of water from confined aquifers, *J. Geophys. Res.*, *84*, 2995–3007.

Catling, D. C., and J. M. Moore (2003), The nature of coarse-grained crystalline hematite and its implications for the early environment of Mars, *Icarus*, *165*, 277–300.

Chan, M. A., W. T. Parry, and J. R. Bowman (2000), Diagenetic hematite and manganese oxides and fault-related fluid flow in Jurassic sandstones, southeastern Utah, *AAPG Bull.*, *84*(9), 1281–1310.

Chan, M. A., B. Beitler, W. T. Parry, J. Ormo, and G. Komatsu (2004), A possible terrestrial analogue for haematite concretions on Mars, *Nature*, *429*, 731–734.

Chapman, M. G., and K. L. Tanaka (2002), Related magma-ice interactions: Possible origins of chasmata, chaos, and surface materials in Xanthe, Margaritifer, and Meridiani Terrae, Mars, *Icarus*, *155*, 324–339.

Christensen, P. R., and S. W. Ruff (2004), The formation of the hematite-bearing unit in Meridiani Planum: Evidence for deposition in standing water, *J. Geophys. Res.*, *109*, E08003, doi:10.1029/2003JE002233.

Christensen, P. R., et al. (1992), Thermal Emission Spectrometer Experiment: Mars Observer Mission, *J. Geophys. Res.*, *97*, 7719–7734.

Christensen, P. R., et al. (2000a), Detection of crystalline hematite mineralization on Mars by the Thermal Emission Spectrometer: Evidence for near-surface water, *J. Geophys. Res.*, *105*, 9623–9642.

Christensen, P. R., J. L. Bandfield, M. D. Smith, V. E. Hamilton, and R. N. Clark (2000b), Identification of a basaltic component on the Martian surface from Thermal Emission Spectrometer Data, *J. Geophys. Res.*, *105*, 9609–9621.

Christensen, P. R., R. V. Morris, M. D. Lane, J. L. Bandfield, and M. C. Malin (2001a), Global mapping of Martian hematite deposits: Remnants of water-driven processes on early Mars, *J. Geophys. Res.*, *106*, 23,873–23,886.

Christensen, P. R., et al. (2001b), Mars Global Surveyor Thermal Emission Spectrometer experiment: Investigation description and surface science results, *J. Geophys. Res.*, *106*, 23,823–23,872.

Christensen, P. R., et al. (2003), Morphology and composition of the surface of Mars: Mars Odyssey THEMIS results, *Science*, *300*, 2056–2061.

Christensen, P. R., et al. (2004a), Mineralogy at Meridiani Planum from the Mini-TES experiment on the Opportunity rover, *Science*, *306*, 1733–1739.

Christensen, P. R., et al. (2004b), The Thermal Emission Imaging System (THEMIS) for the Mars 2001 Odyssey mission, *Space Sci. Rev.*, *110*, 85–130.

Cooper, C. D., and J. F. Mustard (2001), TES observations of the global distribution of sulfate on Mars [CD-ROM], *Lunar Planet. Sci.*, *XXXII*, abstract 2048.

Cooper, C. D., and J. F. Mustard (2002), Spectroscopy of loose and cemented sulfate-bearing soils: Implications for duricrust on Mars, *Icarus*, *158*, 42–55.

Cornell, R. M., and U. Schwertmann (1996), *The Iron Oxides*, 573 pp., VCH, Weinheim, Germany.

De Grave, E., R. Vochten, O. Quenard, E. Van San, H. Desseyn, and A. Rousset (1999), Mössbauer characterization of the products resulting from hydrothermal treatments of nanosized goethite, *Nanostruct. Mater.*, *11*, 493–504.

Edgett, K. S., and M. C. Malin (2002), Martian sedimentary rock stratigraphy: Outcrops and interbedded craters of Northwest Sinus Meridiani and Southwest Arabia Terra, *Geophys. Res. Lett.*, *29*(24), 2179, doi:10.1029/2002GL016515.

Edgett, K. S., and T. J. Parker (1997), Water on early Mars: Possible subaqueous sedimentary deposits covering ancient cratered terrain in western Arabia and Sinus Meridiani, *Geophys. Res. Lett.*, *24*, 2897–2900.

Fallacaro, A., and W. M. Calvin (2003), Spectral and chemical characteristics of Lake Superior banded iron formation: Analog for Martian hematite outcrops, paper presented at Sixth International Conference on Mars, abstract 3067, Lunar and Planet. Inst., Pasadena, Calif.

Gendrin, A., et al. (2005), Sulfates in Martian layered terrains: The OMEGA/Mars Express view, *Science*, *307*, 1587–1590.

Gillespie, A. R., A. B. Kahle, and R. E. Walker (1986), Color enhancement of highly correlated images: I. Decorrelation and HIS contrast stretches, *Remote Sens. Environ.*, *20*, 209–235.

Glotch, T. D., and P. R. Christensen (2003), Geology of Aram Chaos [CD-ROM], *Lunar Planet. Sci.*, *XXXIV*, abstract 2046.

Glotch, T. D., R. V. Morris, and P. R. Christensen (2002), Effect of aluminum substitution on the emissivity spectra of hematite [CD-ROM], *Lunar Planet. Sci.*, *XXXIII*, abstract 1847.

Glotch, T. D., R. V. Morris, P. R. Christensen, and T. G. Sharp (2004), Effect of precursor mineralogy on the thermal infrared emission spectra of hematite: Application to Martian hematite mineralization, *J. Geophys. Res.*, *109*, E07003, doi:10.1029/2003JE002224.

Greenwood, J. P., R. E. Blake, V. Barron, and J. Torrent (2004), P/Fe as an aquamarker for Mars [CD-ROM], *Lunar Planet. Sci.*, *XXXV*, abstract 1839.

Hanna, J. C., and R. J. Phillips (2003), Theoretical modeling of outflow channels and chaos regions on Mars, *Eos Trans. AGU*, *84*(46), Fall Meet. Suppl., Abstract P11B-1036.

Hartmann, W. K., and G. Neukum (2001), Cratering records in the inner solar system in relation to the lunar reference system, *Space Sci. Rev.*, *96*, 55–86.

Hartmann, W. K., J. Anguita, M. A. de la Casa, D. C. Berman, and E. V. Ryan (2001), Martian cratering, 7, The role of impact gardening, *Icarus*, *149*, 37–53.

Head, J. W., III, H. Hiesinger, M. A. Ivanov, M. A. Kreslavsky, S. Pratt, and B. J. Thomson (1991), Possible ancient oceans on Mars: Evidence from Mars Orbiter Laser Altimeter data, *Science*, *286*, 2134–2137.

Herbert, R. B., Jr. (1995), Precipitation of Fe oxyhydroxides and jarosite from acidic groundwater, *GFF*, *117*, 81–85.

Herbert, R. B., Jr. (1997), Properties of goethite and jarosite precipitated from acidic groundwater, Dalarna, Sweden, *Clays Clay Miner.*, *45*, 261–273.

Hynek, B. M. (2004), Implications for hydrologic processes on Mars from extensive bedrock outcrops throughout Terra Meridiani, *Nature*, *431*, 156–159.

Hynek, B. M., R. E. Arvidson, and R. J. Phillips (2002), Geologic setting and origin of Terra Meridiani hematite deposit on Mars, *J. Geophys. Res.*, *107*(E10), 5088, doi:10.1029/2002JE001891.

Jakosky, B. M., and R. J. Phillips (2001), Mars' volatile and climate history, *Nature*, *412*, 237–244.

Jakosky, B. M., M. T. Mellon, H. H. Kieffer, P. R. Christensen, E. S. Varnes, and S. W. Lee (2000), The thermal inertia of Mars from the Mars Global Surveyor Thermal Emission Spectrometer, *J. Geophys. Res.*, *105*, 9643–9652.

Klingelhöfer, G., et al. (2003), Athena MIMOS II Mössbauer spectrometer investigation, *J. Geophys. Res.*, *108*(E12), 8067, doi:10.1029/2003JE002138.

Kirkland, L. E., K. C. Herr, and P. M. Adams (2004), A different perspective for the Mars rover "Opportunity" site: Fine-grained, consolidated hematite and hematite coatings, *Geophys. Res. Lett.*, *31*, L05704, doi:10.1029/2003GL019284.

Komatsu, G., J. S. Kargel, V. R. Baker, R. G. Strom, G. G. Ori, C. Mosangini, and K. L. Tanaka (2000), A chaotic terrain formation hypothesis: Explosive outgas and outflow by dissociation of clathrate on Mars [CD-ROM], *Lunar Planet. Sci.*, *XXXI*, abstract 1434.

Kraft, M. D., J. R. Michalski, and T. G. Sharp (2004), High-silica rock coatings: TES surface-type 2 and chemical weathering on Mars [CD-ROM], *Lunar Planet. Sci.*, *XXXV*, abstract 1936.

Lane, M. D., W. K. Hartmann, and D. C. Berman (2001), Update on studies of the Martian hematite rich-areas [CD-ROM], *Lunar Planet. Sci.*, *XXXII*, abstract 1984.

Lane, M. D., R. V. Morris, S. A. Mertzman, and P. R. Christensen (2002), Evidence for platy hematite grains in Sinus Meridiani, Mars, *J. Geophys. Res.*, *107*(E12), 5126, doi:10.1029/2001JE001832.

Lane, M. D., P. R. Christensen, and W. K. Hartmann (2003), Utilization of the THEMIS visible and infrared imaging data for crater population studies of the Meridiani Planum landing site, *Geophys. Res. Lett.*, *30*(14), 1770, doi:10.1029/2003GL017183.

Langmuir, D. (1971), Particle size effect on the reaction goethite = hematite + water, *Am. J. Sci.*, *271*, 147–156.
Malin, M. C. (1976), Nature and origin of the intracrater plains on Mars, Ph.D. dissertation, Calif. Inst. of Technol., Pasadena.
Malin, M. C., G. E. Danielson, M. A. Ravine, and T. A. Soulanille (1991), Design and development of the Mars Observer Camera, *Int. J. Imag. Syst. Technol.*, *3*, 76–91.
Malin, M. C., G. E. Danielson, A. P. Ingersoll, H. Masursky, J. Veverka, M. A. Ravine, and T. A. Soulanille (1992), Mars Observer Camera, *J. Geophys. Res.*, *97*, 7699–7718.
Masursky, H., J. M. Boyce, A. L. Dial, G. G. Schaber, and M. E. Strobell (1977), Classification and time of formation of Martian channels based on Viking data, *J. Geophys. Res.*, *82*, 4016–4038.
Max, M. D., and S. M. Clifford (2000), The initiation of Martian outflow channels through the catastrophic decomposition of methane hydrate [CD-ROM], *Lunar Planet. Sci.*, *XXXI*, abstract 2094.
Maxwell, T. A., and M. D. Picard (1974), Evidence of subsurface water in equatorial regions of Mars, *AAPG Bull.*, *58*, 915.
Mellon, M. T., B. M. Jakosky, H. H. Kieffer, and P. R. Christensen (2000), High-resolution thermal inertia mapping from the Mars Global Surveyor Thermal Emission Spectrometer, *Icarus*, *148*, 437–455.
Michalski, J. R., M. D. Kraft, T. G. Sharp, L. B. Williams, and P. R. Christensen (2005), Mineralogical constraints on the high-silica Martian surface component observed by TES, *Icarus*, *174*, 161–177.
Milton, J. D. (1974), Carbon-dioxide hydrate and floods on Mars, *Science*, *183*, 654–656.
Morris, R. V., T. G. Graff, S. A. Mertzman, M. D. Lane, and P. R. Christensen (2003), Palagonitic (not andesitic) Mars: Evidence from thermal emission and VNIR spectra of palagonitic alteration rinds on basaltic rock, paper presented at Sixth International Conference on Mars, abstract 3211, Lunar and Planet. Inst., Pasadena, Calif.
Newsom, H. E., C. A. Barber, T. M. Hare, R. T. Schelble, V. A. Sutherland, and W. C. Feldman (2003), Paleolakes and impact basins in southern Arabia Terra, including Meridiani Planum: Implications for the formation of hematite deposits on Mars, *J. Geophys. Res.*, *108*(E12), 8075, doi:10.1029/2002JE001993.
Noreen, E., K. L. Tanaka, and M. G. Chapman (2000), Examination of igneous alternatives to Martian hematite using terrestrial analogs (abstract), *Geol. Soc. Am.*, *32*, A303.
Nummedal, D. (1978), The role of liquefaction in channel development on Mars, Report of the Planetary Geology Program, 1977–1978 (abstract), *NASA Tech. Memo.*, *79729*, 257–259.
Nummedal, D., and D. B. Prior (1981), Generation of Martian chaos and channels by debris flow, *Icarus*, *45*, 77–86.
Ormö, J., G. Komatsu, M. A. Chan, B. Beitler, and W. T. Parry (2004), Geological features indicative of processes related to the hematite formation in Meridiani Planum and Aram Chaos, Mars: A comparison with diagenetic hematite deposits in southern Utah, USA, *Icarus*, *171*, 295–316.
Parker, T. J., R. S. Saunders, and D. M. Schneeberger (1989), Transitional morphology in West Deuteronilus Mensae, Mars: Implications for modification of the lowland/upland boundary, *Icarus*, *82*, 111–145.
Parker, T. J., D. S. Gorsline, R. S. Saunders, D. C. Pieri, and D. M. Schneeberger (1993), Coastal geomorphology of the Martian northern plains, *J. Geophys. Res.*, *98*, 11,061–11,078.
Pepin, R. O. (1994), Evolution of the Martian atmosphere, *Icarus*, *111*, 289–304.
Pollack, J. B., J. F. Kasting, S. M. Richardson, and K. Poliakoff (1987), The case for a warm wet climate on early Mars, *Icarus*, *71*, 203–224.
Presley, M. A., and P. R. Christensen (1997), Thermal conductivity measurements of particulate materials: 2, Results, *J. Geophys. Res.*, *102*, 6551–6556.
Ramsey, M. S., and P. R. Christensen (1998), Mineral abundance determination: Quantitative deconvolution of thermal emission spectra, *J. Geophys. Res.*, *103*, 577–596.
Rogers, D., P. R. Christensen, and J. L. Bandfield (2005), Compositional heterogeneity of the ancient Martian crust: Analysis of Ares Vallis bedrock with THEMIS and TES data, *J. Geophys. Res.*, *110*, E05010, doi:10.1029/2005JE002399.
Rotto, S., and K. L. Tanaka (1991), Geologic history and channeling episodes of the Chryse Planitia region of Mars, *Lunar Planet Sci.*, *XXII*, 1135–1136.
Rotto, S., and K. L. Tanaka (1995), Geologic/geomorphic map of the Chryse Planitia region of Mars, *U.S. Geol. Surv. Misc. Invest. Ser. Map, I-2441*.
Ruff, S. W. (2004), Spectral evidence for zeolite in the dust on Mars, *Icarus*, *168*, 131–143.
Ruff, S. W., P. R. Christensen, R. N. Clark, H. H. Kieffer, M. C. Malin, J. L. Bandfield, B. M. Jakosky, M. D. Lane, M. T. Mellon, and M. A. Presley (2001), Mars' "White Rock" feature lacks evidence of an aqueous origin: Results from Mars Global Surveyor, *J. Geophys. Res.*, *106*(E10), 23,921–23,928.
Schultz, P. H., R. A. Schultz, and J. R. Rogers (1982), The structure and evolution of ancient impact basins on Mars, *J. Geophys. Res.*, *87*, 9803–9820.
Sharp, R. P. (1973), Mars: Fretted and chaotic terrains, *J. Geophys. Res.*, *78*, 4073–4083.
Sharp, R. P., L. A. Soderblom, B. C. Murray, and J. A. Cutts (1971), The surface of Mars, 2 uncratered terrains, *J. Geophys. Res.*, *76*, 331–342.
Smith, D. E., et al. (2001), Mars Orbiter Laser Altimeter: Experiment summary after the first year of global mapping of Mars, *J. Geophys. Res.*, *106*, 23,689–23,722.
Smith, M. D., J. L. Bandfield, and P. R. Christensen (2000a), Separation of atmospheric and surface spectral features in Mars Global Surveyor Thermal Emission Spectrometer (TES) spectra, *J. Geophys. Res.*, *105*, 9589–9607.
Smith, M. D., J. C. Pearl, B. J. Conrath, and P. R. Christensen (2000b), Mars Global Surveyor Thermal Emission Spectrometer (TES) observations of dust opacity during aerobraking and science phasing, *J. Geophys. Res.*, *105*, 9539–9552.
Soderblom, L. A., et al. (2004), Soils of Eagle Crater and Meridiani Planum at the Opportunity Rover landing site, *Science*, *306*, 1723–1726.
Squyers, S. W., et al. (2004), In situ evidence for an ancient aqueous environment at Meridiani Planum, Mars, *Science*, *306*, 1709–1713.
Stahl, R. S., D. S. Fanning, and B. R. James (1993), Goethite and jarosite precipitation from ferrous sulfate solutions, *Soil. Sci. Soc. Am. J.*, *57*, 280–282.
Tanaka, K. L. (1988), Chaotic material and debris flows in the Simud/Tiu Valles outflow system of Mars, *Lunar Planet. Sci.*, *19*, 1175–1176.
Tanaka, K. L. (1999), Debris-flow origin for the Simud/Tiu deposit on Mars, *J. Geophys. Res.*, *104*, 8637–8652.
Tanaka, K. L., and J. A. Skinner Jr. (2004), Advances in reconstructing the geologic history of the Chryse region outflow channels on Mars [CD-ROM], *Lunar Planet. Sci.*, *XXXV*, abstract 1770.
Tanaka, K. L., B. W. Banerdt, J. S. Kargel, and N. Hoffman (2001), Huge, CO2–charged debris-flow deposit and tectonic sagging in the Northern Plains of Mars, *Geology*, *29*, 427–430.
Tanaka, K. L., J. A. Skinner Jr., T. M. Hare, T. Joyal, and A. Wenker (2003), Resurfacing history of the northern plains of Mars based on geologic mapping of Mars Global Surveyor data, *J. Geophys. Res.*, *108*(E4), 8043, doi:10.1029/2002JE001908.
Wyatt, M. B., and H. Y. McSween Jr. (2002), Spectral evidence for weathered basalt as an alternative to andesite in the northern lowlands of Mars, *Nature*, *417*, 263–266.
Wyatt, M. B., V. E. Hamilton, H. Y. McSween Jr., P. R. Christensen, and L. A. Taylor (2001), Analysis of terrestrial and Martian volcanic compositions using thermal emission spectroscopy: 1. Determination of mineralogy, chemistry, and classification strategies, *J. Geophys. Res.*, *106*, 14,711–14,732.
Zuber, M. T., D. E. Smith, S. C. Solomon, D. O. Muhleman, J. W. Head, J. B. Garvin, J. B. Abshire, and J. L. Bufton (1992), The Mars Observer Laser Altimeter investigation, *J. Geophys. Res.*, *97*, 7781–7797.

P. R. Christensen and T. D. Glotch, Department of Geological Sciences, Arizona State University, Tempe, AZ 85287-6305, USA. (tglotch@asu.edu)